TITLE:

Massively Parallel Polyribosome Profiling Reveals Translation Defects of Human Disease-Relevant UTR Mutations

Author list:

Wei-Ping Li[1,2,4], Jia-Ying Su[1,3,4], Yu-Chi Chang[1], Hung-Lun Chiang[1], Yun-Lin Wang[1], Ang-Chu Huang[1], Yu-Tung Hsieh[1], Yi-Hsuan Chiang[1], Yen-Ling Ko[1], Bing-Jen Chiang[1], Cheng-Han Yang[1], Yen-Tsung Huang[3], Chien-Ling Lin[1]*

Affiliations:

[1]Institute of Molecular Biology, Academia Sinica, Taipei 115, Taiwan
[2]Department of Complex Trait Genetics, Center for Neurogenomics and Cognitive Research, Vrije Universiteit Amsterdam, Amsterdam, The Netherlands
[3]Institute of Statistical Science, Academia Sinica, Taipei 115, Taiwan
[4]These authors contributed equally

***To whom correspondence should be addressed.**

Email: mbcllin@gate.sinica.edu.tw

Fax: 886-2-2782-6085

Present Address: Institute of Molecular Biology, Academia Sinica, No. 128, Sec. 2, Academia Road, Nangang District, Taipei City 115014, TAIWAN

Keywords: untranslated region, UTR variants, massively parallel reporter assay, polyribosome profiling, RNA translation efficiency

ABSTRACT

The untranslated regions (UTRs) of mRNAs harbor regulatory elements influencing translation efficiency. Although 3.7% of disease-relevant human mutations occur in UTRs, their exact role in pathogenesis remains unclear. Through metagene analysis, we mapped pathogenic UTR mutations to regions near coding sequences, with a focus on the upstream open reading frame (uORF) initiation site. Subsequently, we utilized massively parallel poly(ribo)some profiling to compare the ribosome associations of 6,555 pairs of wildtype and mutant UTR fragments. We identified 46 UTR variants that altered polysome profiles, with enrichment in pathogenic mutations. Both univariate analysis and the elastic net regression model highlighted the significance of motifs of short repeated sequences, including SRSF2 binding sites, as mutation hotspots that lead to aberrant translation. Furthermore, these polysome-shifting mutations exhibited considerable impact on RNA secondary structures, particularly for upstream AUG-containing 5' UTRs. Integrating these features, our model achieved high accuracy (AUROC > 0.8) in predicting polysome-shifting mutations in the test dataset. Additionally, several lines of evidence indicate that changes in uORF usage underlie the translation deficiency arising from these mutations. Illustrating this, we demonstrate that a pathogenic mutation in the IRF6 5' UTR suppresses translation of the primary open reading frame by creating a uORF. Remarkably, site-directed ADAR editing of the mutant mRNA rescued this translation deficiency. Overall, our study provides insights into the molecular mechanisms of UTR mutations and their links to clinical impacts through translation defects.

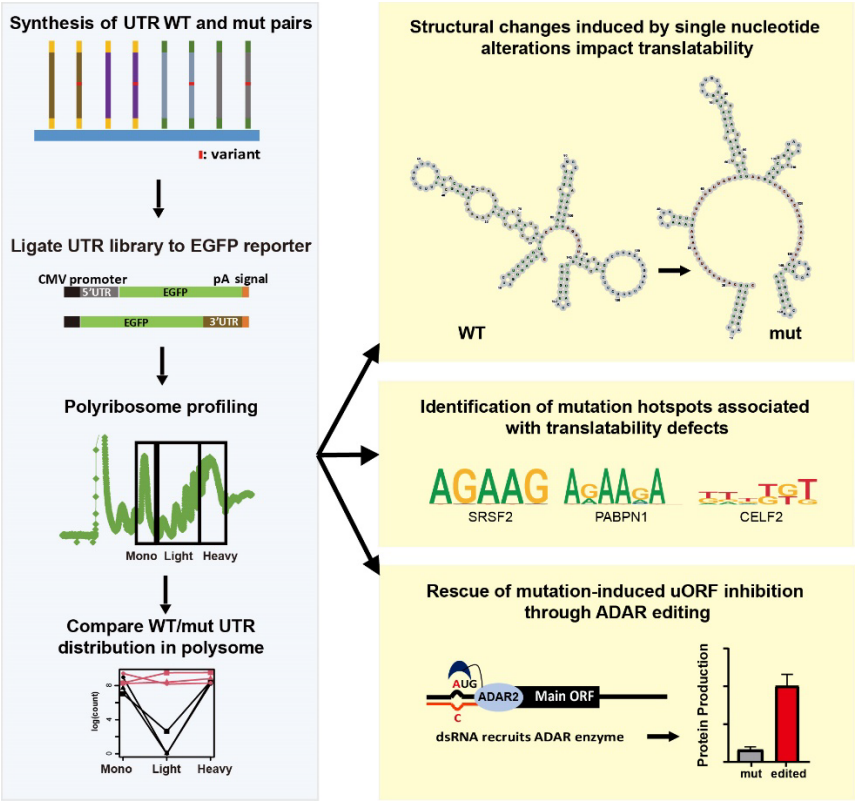

INTRODUCTION

Untranslated regions (UTRs) control translation efficiency

UTRs are crucial to gene expression regulation. Whilst mRNA coding regions determine protein sequence, the UTRs modulate protein abundance via, for instance, tuning stability and translation of mRNAs thereof. Many studies have shown that structural elements in 5' UTRs are involved in translation regulation. An iron regulatory protein (IRP) that maintains iron homeostasis binds to an iron-responsive element (IRE) in the 5' UTR of ferritin mRNAs, blocks recruitment of translation initiation factors, and elicits translation inhibition (Klausner et al., 1993; Muckenthaler et al., 1998). Internal ribosome entry sites (IRESs) are another *cis*-acting element of 5' UTRs that control translation. IRESs in 5' UTRs facilitate translation initiation by presenting ribosome-binding sites in a 5' cap-independent manner (Komar & Hatzoglou, 2005). On the contrary, guanine-quadruplex motifs, which can adopt a non-canonical secondary structure in the 5' UTR, are known to repress translation (Kumari et al., 2007; Serikawa et al., 2018). On the other hand, although 3' UTRs lie far from the translation initiation site, they can regulate translation efficiency by controlling polyadenylation and binding of *trans*-acting factors. For instance, the poly(A) tail of mRNA can loop with its 5' end, facilitating translation and ribosome recycling (Choe et al., 2018; Wells et al., 1998). Moreover, proteins and miRNAs that are deposited on 3' UTRs can regulate various phases of translation including initiation, elongation, and termination (Mazumder et al., 2003).

Massively parallel translation assays

To decode the regulatory potential of UTRs, we developed a massively parallel reporter assays (MPRAs), in which UTRs of fixed length adjoin the coding sequence of a reporter. Similar approaches have been adopted to reveal the sequence-specific regulation and modular functions of numerous processes, including transcription, RNA splicing, translation, RNA localization, RNA decay and protein degradation in various species (Abell et al., 2022; Chiang et al., 2022; Griesemer et al., 2021; Jia et al., 2020; Litterman et al., 2019; Mikl et al., 2022; Niederer et al., 2022; Oikonomou et al., 2014; Rabani et al., 2017; Sample et al., 2019; Savinov et al., 2021; Slutskin et al., 2018; Zhao et al., 2014). In some studies of RNA translation, reporter protein output, for example, intensity of the green fluorescent protein (GFP), has been used as a readout of regulatory activity. However, protein output essentially is the product of the interaction between RNA half-lives and its translatability. Therefore, for a more unequivocal study design, poly(ribo)some profiling has been used to estimate RNA translatability through evaluating their ribosome association status. MPRA based on polyribosome profiling technique has been applied to examine the translational efficiency of UTRs of interest. For instance, it has been shown previously that variations in 5' UTRs have a greater impact on ribosome load than those in coding regions or 3' UTRs (Leppek et al., 2022). MPRAs on 5' UTRs have demonstrated that an upstream start codon (uATG) or open reading frame (uORF) can suppress primary ORF translation (Jia et al., 2020; Sample et al., 2019). Structural hindrances, such as RNA G-quadruplexes (RG4) and stem-loops, also can suppress translation (Fay et al., 2017; Jia et al., 2020; Leppek et al., 2022). Additionally, at the sequence level, G-rich and C-rich elements are repressors of translation, whereas A-rich elements enhance translation (Jia et al., 2020; Niederer et al., 2022). Most massively parallel polysome profiling studies exclusively examined 5' UTRs, likely due to the general assumption that 5' UTRs play the major role in ribosome recruitment. On the other hand, MPRAs assessing fluorescent protein expression showed that binding sites for miRNAs and RNA-binding proteins (RBPs), particularly AU-rich elements, played a critical role in regulating the

protein output (Oikonomou et al., 2014; Stoecklin et al., 2001; Wissink et al., 2016). Pumilio and AU-rich element-binding proteins, such as Tristetraprolin (TTP) and the embryonic lethal abnormal vision (ELAV) family, have been shown to influence protein expression (Barreau et al., 2005; Mayya & Duchaine, 2019; Van Etten et al., 2012). Nevertheless, whether these RBP or miRNA binding sites dampened protein level via impeding ribosome association was not corroborated by those MPRA studies.

Precision diagnosis of UTR mutations

The genetic variants in UTRs may affect mRNA stability, translation, and localization, which in turn impact the flow of gene expression and hence result in phenotypical change and even pathogenesis. Prior studies have evidenced that even single nucleotide changes in a UTR can affect mRNA translation and/or transcript half-life in disease contexts. For example, single nucleotide substitutions at the 36th position of the 5' UTR or the 1723rd position and the 3' UTR of transforming growth factor β3 (TGFβ3; MIM# 190230) are associated with typical arrhythmogenic right ventricular cardiomyopathy (Beffagna et al., 2005). Another such example is a point mutation in the 3' UTR of glutamine-fructose-6-phosphate transaminase 1 (GFPT1), which results in congenital myasthenic syndrome. GFPT1 is a rate-limiting enzyme for hexosamine biosynthesis, and a mutation in its 3' UTR has been known to cause 90% reduction in protein production, potentially due to gain of a miRNA binding site (Dusl et al., 2015). All things considered, sequence integrity of UTRs has profound effects on gene regulation, given that variants in UTRs may induce various phenotypes and even lead to severe diseases.

To systematically evaluate the impact of disease-relevant UTR variants on translation, we employed massively parallel ribosome profiling on both 5' and 3' UTRs to examine the effects of mutations on ribosome association. Through this strategy, we identified 46 high-confidence variants that caused ribosome shifting, and, intriguingly, their functional consequences converged on changes of RNA secondary structure and RBD binding motifs. Moreover, we investigated the molecular mechanism of a severe 5' UTR suppressive mutation and developed ADAR-based editing to rescue the expression defect.

MATERIAL AND METHODS

Metagene analysis

All UTR and uORF variants were assigned using dbSNP version 151 (Sherry et al., 1999), with disease variants and UTR sources as described above. Definitions of uORFs were downloaded from TIS-db (Wan & Qian, 2014), and the respective genome coordinates were lifted from the Genome Reference Consortium hg19 to hg38 before analysis.

Variant collection

Disease-related variants were collected from ClinVar (Landrum et al., 2016) and the HGMD database (Stenson et al., 2017). Variants located in the coding region or labeled as benign variants were excluded. UTRs were defined using NCBI RefSeq and ENCODE V27. Then, we intersected selected variant positions with the UTR regions by using BEDTools (Quinlan & Hall, 2010) to collect UTR variants.

Construction of a UTR library of DNA templates

A UTR library of DNA templates was assembled by overlapping extension polymerase chain reaction (PCR) using Herculase II Fusion Enzyme (Agilent Technologies). Initially, the oligonucleotide library sequences (CustomArray Inc., USA) were double-strandized and amplified by PCR. After PCR clean-up (Qiagen), the UTR library amplicons were appended sequentially with EGFP CDS and CMV promoter sequences (derived from EGFP-N1 vector) by means of overlapping PCR. The assembled full-length DNA templates (CMVP-5'UTR-EGFP or CMVP-EGFP-3'UTR) were subjected to PCR clean-up for subsequent transfection. Primers are listed in Supplemental Table S1.

Polysome fractionation and preparation for next generation sequencing

Polysome fractionation was conducted in accordance with a protocol published previously (Gandin et al., 2014) with slight modification. In brief, HEK293T cells cultured in 15-cm Petri dishes were grown to 60-70% confluency and then transfected with 4 µg of the UTR library of DNA templates (2 µg for each UTR library) using lipofectamine 3000 reagent (Invitrogen). Fourteen hours after transfection, the cells were incubated in culture medium containing 100 µg/ml cycloheximide (CHX) (Sigma) for 5 minutes. Subsequently, the cells were washed twice with and then detached in ice-cold 1x PBS containing 100 µg/ml CHX, followed by centrifugation at 200 x *g* for 5 minutes at 4 °C. The entire procedure was conducted at a low temperature with the addition of 100 µg/ml CHX to preserve the polysome status. After discarding the supernatant, the cell pellet was re-suspended with 425 µl of hypotonic buffer (5 mM Tris-HCl (pH 7.5), 2.5 mM $MgCl_2$, 1.5 mM KCl and 1x EDTA-free protease inhibitor cocktail (Roche)). Next, 5 µl of 10 mg/ml CHX, 1 µl of 1 M DTT, and 100 units of RNase inhibitor (Invitrogen) were added into the cell suspension, followed by vortexing for 5 seconds. Then, 25 µl of 10% Triton X-100 and 25 µl of 10% Sodium Deoxycholate were added into the suspension. After lysing the cells on ice for 5 minutes, the lysate was centrifuged at 16,000 x *g* for 7 minutes at 4 °C. The supernatant was collected and then layered onto a 5-50% sucrose gradient made of 5% and 50% sucrose solutions containing 20 mM HEPES (pH 7.6), 0.1 M KCl, 5 mM $MgCl_2$, 10 µg/ml CHX, 0.1x EDTA-free protease inhibitor cocktail, and 10 units/ml RNase inhibitor, before undergoing ultracentrifugation with a SW41 Ti rotor (Beckman Coulter) at 36,000 rpm and 4 °C for 2 hours. Afterwards, the gradient samples were fractionated by fixed volume (500 µl/fraction), and all of the fractions were collected and subjected to RNA extraction (Direct-zol™ RNA MiniPrep Plus, Zymo Research). In addition to the indication of polysome profile derived from UV absorbance, the identity of each fraction was further verified through examining the distribution of 18S and 28S rRNAs among fractions via RNA electrophoresis.

Next, fractions corresponding to ribosome peaks were further categorized into three groups: monosome (Mono), low-density polysome (Light, 2-5 ribosomes), and high-density polysome (Heavy, ≥ 6 ribosomes). Then, the RNAs extracted from the fractions corresponding to each group were pooled together in an equal-fraction manner and subjected to reverse transcription using SuperScript IV First-Strand Synthesis System (Invitrogen). Thereafter, the UTR regions of mRNAs derived from our UTR library of DNA templates were amplified from the cDNA products using Phusion PCR Master Mix/GC Buffer (Thermo) and primers hosting Illumina sequencing adaptors and random tri-nucleotides for Illumina® NextSeq paired-end 150 sequencing.

RNA sequencing analysis

The Illumina NextEra adapter CTGTCTCTTATACACATCT and low quality bases (sliding mean quality < 20) were removed from the raw fastq using trimmomatic (Bolger et al., 2014). The qualified reads were then aligned to the reference library with hisat2 (Smith et al., 2017), and sorted by samtools (Danecek et al., 2021):

```
hisat2 --mp 1,1 --rdg 1,1 -x indexFile -U fastq_R1.gz | samtools sort -o out_sorted.bam
```

After sorting, the "Exactly One Time Alignment" filter was applied to the results by samtools view command with the -q 60 parameter and the output index bam file was generated by samtools index command. A final raw count table was built using the *multicov* command in BEDTools (Quinlan & Hall, 2010).

Statistical method for detecting the effect of mutations on polysome profiles

To determine variants that changed polysome distribution, we used read counts in polysome fractions to build a negative binomial generalized linear model with a log link function for each pair of oligonucleotides as follows:

$$\ln(C_i) = \beta_0 + \beta_F F_i + \beta_E E_i + \beta_G G_i + \theta G_i F_i + \eta G_i E_i$$

where C_i are read count values of the ith replicate, F_i represents the three polysome fractions (Mono, Light and Heavy), E_i represents biological replicates, and G_i represents WT or mutant.

We tested the significance of θ to determine the effect of the variant. To avoid potential batch effects, we further excluded candidates with significant η or β_E ($p < 0.05$).

All statistical analyses were performed using R language (version 4.2.2). Linear models were constructed using the *glm.nb* function in R.

Construction of DNA templates for luciferase assay

Linear constructs (CMVP-5'UTR-FFLuc or CMVP-FFLuc-3'UTR) for luciferase assay were assembled by overlap extension PCR using Phusion DNA Polymerase (Thermo). Initially, DNA oligos (Integrated DNA Technologies Inc.) of selected UTR candidate sequences were double-strandized and amplified by PCR. Afterwards, the purified UTR amplicons were appended with firefly luciferase CDS (derived from pGL3-Basic vector) and the CMV promoter sequence (derived from EGFP-N1 vector) sequentially via overlapping PCR.

Luciferase assay, RNA extraction, and RT-qPCR

Fourteen to fifteen hours after co-transfection with 500 ng of linear constructs (CMVP-5'UTR-FFLuc or CMVP-FFLuc-3'UTR) and 100 ng of pRL-TK vector, HEK293T cells cultured in a 12-well plate were harvested and processed according to the instruction of Dual-Glo Luciferase Assay System (Promega) with minor modification. In brief, after removing media and washing once with PBS, the transfected cells were detached and then lysed in 180 µl of Dual-Glo reagent, before being subjected to moderate shaking on an orbital shaker at room temperature for 10 minutes. The lysate was then transferred to a new tube and underwent low-speed centrifugation to remove the cell debris. Then, 50 µl of clear supernatant was transferred to 96-well black plates to measure firefly luminescence with EnSpire Multimode Plate Reader (PerkinElmer) or SpectraMax Paradigm reader (Molecular Devices) and the software SoftMax Pro. Subsequently, 50 µl of Dual-

Glo Stop & Glo Reagent was added into each well. After incubation at room temperature for 10 minutes, *Renilla* luminescence was measured as above.

Relative luminescence units (RLUs) were calculated by dividing the firefly luciferase readouts by those of the transfection control, i.e., *Renilla* luciferase. To evaluate translation efficiency, the RLUs were normalized to the transcript level measured by real-time PCR. Apart from those specifically annotated herein, all data is shown as the fold-change of the mutant relative to wildtype.

To calibrate the luciferase assay results against cognate mRNA expression level, total RNAs were extracted from the cells subjected to identical transfection conditions with TRIzol reagent (Invitrogen). Total RNA was extracted with Direct-zol RNA Miniprep kits (Zymo Research), before being subjected to reverse transcription. Then, cDNA was reverse-transcribed from 1 µg of RNA using 2.5 µM random hexamer with 1 µl (200U) SuperScript IV Reverse Transcriptase (Thermo Scientific). The reaction mixture was incubated at 24°C for 10 min to allow primer annealing, followed by incubation at 50°C for 10 min for reverse transcription. Subsequently, the reaction was terminated by incubating at 80°C for 10 min to inactivate the reverse transcriptase. Finally, the cDNA products were subjected to real-time PCR with Fast SYBR Green Master Mix (QuantStudio 12K Flex system, Applied Biosystems) to determine the expression level of firefly luciferase relative to that of *Renilla* luciferase.

Motif enrichment analysis

Motif analysis including RBP position weight matrix (PWM), K-mer and miRNA seed sequence. RBP PWM definitions were downloaded from the ATtRACT database (Giudice et al., 2016). For each UTR sequence, all possible motif PWMs were determined using the R package Biostrings (Pagès H, 2022) and the *matchPWM*() function with the parameter min.score = 95%. To summarize the contribution of each RBP, PWMs predicted for the same RBP gene were summed. K-mer composition was determined in Biostrings using the *oligonucleotideFrequency*() function, with K-mer lengths of 1 to 7. miRNA binding sites were predicted in TargetScan 7.0 (Agarwal et al., 2015), with high-confidence predictions (8mer, 7mer-m8, 7mer-1A) for each miRNA being summed to represent counts of the seed sequence.

To find motifs enriched in UTRs of interest, motif distribution in relation to UTRs was analyzed by Fisher's exact test using the *fisher.tes*t() function in R (R-Core-Team, 2021) according to the matrix:

$$\begin{bmatrix} count\ of\ motif[i]\ \in\ sig\ UTRs & count\ of\ motif[i]\ \in\ nonsig\ UTRs \\ all\ motif\ count\ \in\ sig\ UTRs & all\ motif\ count \in\ nonsig\ UTRs \end{bmatrix}$$

To examine motif changes in relation to polysome shifting, motifs disrupted by variants and the resulting shift in polysomes was analyzed by using the *fisher.tes*t() function in R according to the matrix:

$$\begin{bmatrix} sig\ UTRs\ with\ motif[i]\ change & nonsig\ UTRs\ with\ motif[i]\ change \\ sig\ UTRs\ without\ motif[i]\ change & nonsig\ UTRs\ without\ motif[i]\ change \end{bmatrix}$$

shRNA-mediated knockdown

For shRNA expression, pLKO.1 vectors containing an shRNA sequence (5'-AGTTGTGTAGCAGTTGAGTAA-3') targeting the human *SRSF2* 3' UTR or a non-targeting scrambled control (5'-CCTAAGGTTAAGTCGCCCTCG-3') were obtained from the RNAi Core, Academia Sinica, Taiwan, and lentiviral particles were produced using HEK293T cells by following standard procedures.

The HEK293T cells were initially seeded at a density of $5x10^5$ cells per well in 6-well plates. Four hours after seeding, shRNA-expressing lentivirus was introduced into the HEK293T cells at a multiplicity of infection (MOI) of 5. Then, the virus-containing medium was replaced after 24-hour incubation with 2 ml of DMEM supplemented with 10% FBS. Following an additional 24-hour incubation, the culture medium was supplemented with 2.5 µg/ml puromycin for selection purposes. The cells underwent a 4-day puromycin selection with one round of medium refreshment. The cells were then incubated in medium with 5 µg/ml puromycin for an additional day. After the selection process, the cells were transferred to a 10 cm dish for expansion and subsequent experiments.

Plasmid construction

For the firefly luciferase reporter plasmids, full-length UTRs were PCR-amplified from HEK293T complementary DNA (cDNA) with Phusion High-Fidelity DNA Polymerase (Thermo Scientific). Restriction enzyme cutting sites (*HindIII* and *NcoI* for 5 'UTRs, *XbaI* for 3' UTRs) were attached for digestion with Thermo Scientific FastDigest kit and for cloning with Rapid DNA Ligation kit (Thermo Scientific) into the pGL3-Promotor (Promega) backbone. Mutants were generated by mutagenesis PCR from wildtype constructs and the same cutting sites as for cloning were adopted.

For motif validation, the 5' UTR sequence of *MUTYH* (mutY DNA glycosylase:c.-43~-157) and the 3' UTR sequence of *MEFV* (Mediterranean fever:c.*17~131) were used, respectively, as the backbone of wildtype UTRs. Motifs were inserted into the *Xba1* site of the *MUTYH* 5' UTR and the *Nhe1* site of the *MEFV* 3' UTR.

For IRF6 ar151-expressing plasmids, the 151 bp antisense sequence with a mismatch in the center was PCR-amplified from wildtype luciferase plasmids. The PCR product was inserted into the pHE vector (BIOTOOLS) and transcription was driven by the human U6 promoter.

UTR secondary structure prediction

UTR secondary structures were predicted and plotted using the forna website (http://rna.tbi.univie.ac.at/forna/) (Kerpedjiev et al., 2015). Free energy was estimated using the viennaRNA package (Lorenz et al., 2011) and the *RNAfold* command with the default setting.

$$\begin{bmatrix} sig\ UTRs\ with\ motif[i]\ change & nonsig\ UTRs\ with\ motif[i]\ change \\ sig\ UTRs\ without\ motif[i]\ change & nonsig\ UTRs\ without\ motif[i]\ change \end{bmatrix}$$

Elastic net model of polysome-shifting UTR variants

To develop a prediction model for determining whether a genetic variant affects mRNA translation, we employed a logistic regression model with elastic net regularization for feature selection. The curated features included free energy, structure rate, GC content, k-mer, G-quadruplex (RG4), conservation level, miRNA binding motif, PUM motif, RBP motif, and ARE.

Before feature selection, the features were narrowed down using multiple logistic regression models to regress the significance of variants (Yes/No) on each feature, with a *p-value* < 0.01 serving as the criterion for identifying potential candidates. Subsequently, the dataset was divided into two groups, comprising training and testing sets in a 2:1 ratio, respectively. The model is represented as follows:

$$\ln\left(\frac{\mathrm{P}(Y_i = 1)}{1 - \mathrm{P}(Y_i = 1)}\right) = \beta_0 + \sum_{j=1}^{p} \beta_j X_{ji}$$

where Y_i = 1 is the ith mt sequence that significantly affects mRNA translation, and X_{ji} is the feature j in the i th sequence. The predictive features were standardized using Z-score transformation to achieve unit standard deviation, thereby ensuring comparability of coefficients. Elastic net regularization minimizes $\mathrm{L}_{\log} + \lambda\left(\frac{1-\alpha}{2}\sum_{j=1}^{p}\beta_j^2 + \alpha\sum_{j=1}^{p}|\beta_j|\right)$, where the negative log likelihood is:

$$\mathrm{L}_{\log} = -\sum_{i=1}^{n}\left[-\ln\left(1 + e^{\left(\beta_0 + \sum_{j=1}^{p}\beta_j X_{ji}\right)}\right) + y_i(\beta_0 + \sum_{j=1}^{p}\beta_j X_{ji})\right]$$

We applied 10-fold cross-validation on the training set to optimize the tuning parameters (λ and α) for the elastic net model. Following this, predictions were made on the testing set to evaluate the model's performance, and the area under the receiver operating characteristic (AUROC) was calculated. Feature selection and AUROC calculations were conducted using the R packages 'caret' (v.6.0.94) and 'precrec' (v.0.14.4) (Kuhn, 2008; Saito & Rehmsmeier, 2017), respectively, with all analyses performed on R version 4.3.3. The 95% confidence intervals for the AUROC values were estimated through bootstrap resampling with 1,000 iterations.

Validation of the elastic net model

To further validate the predictive performance of our elastic net model, we conducted external validation using an independent dataset published by Sample et al. (2019). This dataset comprises curated human 5' UTR sequences that were systematically evaluated using a massively parallel translation assay to assess their effects on translation efficiency (Sample et al., 2019). The dataset was obtained from the authors' publicly available repository (https://github.com/pjsample/human_5utr_modeling).

Prior to analysis, rigorous quality control measures were implemented to ensure data reliability. Sequences were included only if they met the following criteria: an average read count of at least 50 reads per polysome fraction and a minimum of 10 reads in each individual fraction. Since our predictive model outputs binary classifications (significant effect versus no significant effect), we established a threshold to categorize the continuous MRL change values from the Sample et al. dataset. Variants with an absolute $\log_2$ mean ribosome loading (MRL) change of ≥1.0 (corresponding to the "log_obs_diff" column in their dataset) were classified as having significant translational impact, while those below this threshold were considered non-significant. Model performance on the external dataset was evaluated by calculating the AUROC with 95% confidence interval using the same methodology described previously.

It should be noted that external validation for the 3' UTR predictive model could not be performed due to the absence of suitable independent datasets with comparable experimental design and quality standards.

Western blotting

To validate translation activity on the mutant-generated upstream AUG, HEK293T cells were cultured in 6-well plates. After 24 hours, the cloned reporter plasmids and the control pEGFP-N1 were co-transfected by Lipofectamine 3000 (Invitrogen) at a ratio of 3:1 (2.5 µg in total). At 24 h post-transfection, cells were lysed in RIPA buffer (Sigma-Aldrich) supplemented with cOmplete Protease Inhibitor Cocktail (Roche). The solution was transferred onto ice for incubation for 5 minutes and then centrifuged at full speed for 10 minutes at 4 °C. Finally, the supernatant was transferred to a new tube. After determining protein concentration by Bradford assay (Bio-Rad), 30-80 µg of protein sample was loaded into each well. Protein samples separated by sodium dodecyl sulfate-polyacrylamide gel electrophoresis were transferred to PVDF membrane for antibody incubation and ECL detection. Immunoblotting of IRF6: primary antibody against IRF6 (Cell Signaling Technology, Cat# 6948, dilution: 1:1000) and secondary antibody (Jackson ImmunoResearch, Cat#: 111-035-003, 1:5000); Immunoblotting of tubulin: primary antibody against tubulin (Sigma, Cat#: T6793, 1:2000) and secondary antibody (Cell Signaling Technology, Cat#: 7076, 1:5000); Immunoblotting of firefly luciferase: primary antibody against luciferase (Abcam, Cat#: ab185924, 1:1000) and secondary antibody (Abcam, Cat#: ab6721, 1:5000); Immunoblotting of GFP: primary antibody against GFP (ProteinTech, Cat#: HRP-66002, 1:10000).

ADAR editing

HEK293T cells were cultured in 24-well plates. After 24 hours, 200 ng of the reporter plasmids, 20 ng of the pRL-TK plasmids, 150 ng of the ar151 plasmids, and 150 ng of the ADAR2 overexpression plasmids were co-transfected with Lipofectamine 3000 (Invitrogen). Luciferase assays and evaluations of mRNA levels were performed as described above after 40 hours of transfection.

To evaluate the editing efficiency of IRF6 ar151, the cDNA synthesized for qPCR analysis was PCR-amplified with primers targeting 151 bp of the 5’ UTR. PCR products were purified with QIAquick PCR Purification Kit (QIAGEN) according to the manufacturer’s protocol. Elution products were subjected to Sanger sequencing to analyze editing efficiency.

RESULTS

Meta-analysis of disease-relevant UTR variants

It has been estimated that ~3.7% of disease-relevant genetic variants arise in UTRs (MacArthur et al., 2017; Steri et al., 2018). To investigate if there is a positional effect of disease-relevant UTR variants, we compared the overall distribution of disease-associated single nucleotide polymorphisms (SNPs) in ClinVar (Landrum et al., 2016) to over a million human UTR SNPs in the dbSNP archive, which revealed enrichment for disease-relevant variants near mRNA coding regions in both 5’ and 3’ UTRs **(Fig. 1A)**, indicating that the near-coding region of UTRs is a critical regulatory region for gene expression. Although we did not detect enrichment for disease-relevant 5' UTR variants near the transcription start site, they did exist at uORF start sites **(Fig. 1B)**. This specific localization of disease-relevant UTR variants evidences a trend in the positioning of functional elements within UTRs.

Massively parallel poly(ribo)some assays on human disease-relevant UTR mutations

Although many disease-associated UTR variants are located in functional elements, their pathogenic mechanisms remain unknown. To examine if these variants directly affect protein output, we first sought to determine the impact of these variants on translation. To systematically examine the altered translation efficiency by UTR variants, we implemented massively parallel polysome assays to examine the effects of variants on polysome association **(Fig. 2A)**. First, we extracted 6,555 disease-associated UTR variants, including SNPs and indels shorter than 15 nucleotides (nt), from the Human Gene Mutation Database (HGMD) and ClinVar, followed by multiplex oligonucleotide synthesis for selected UTRs. We prioritized UTR variants designated as pathogenic or likely pathogenic in the database. Consequently, all annotated pathogenic and likely pathogenic UTR variants reported by the time of data collection were included in the library. Additionally, due to the constraint of synthesis length (~150 nt), we synthesized the segment of selected UTRs (~115 nt) in which variants were located at the center to maximize the possibility of including critical regulatory elements. Moreover, UTR fragments of both alternative and reference alleles were synthesized in parallel for case-control comparison. In cases where multiple alternative alleles existed at the same position, they were paired with the same reference allele to prevent duplication in the library. The entire library of UTR oligonucleotides (UTR library) was subsequently ligated upstream or downstream of an enhanced GFP (EGFP) coding region, along with a CMV promoter and a common UTR sequence on the opposite end. Cells transfected with the UTR library were treated with cycloheximide 14 hours post transfection and then subjected to polysome fractionation (see Methods). By matching the UV absorbance profile of fractions to rRNA abundance revealed by gel electrophoresis of RNA samples (total RNA extracted from polysome fractions), we were able to estimate the number of bound ribosomes in the collected fractions. RNA samples from fractions containing 1 ribosome, 2 – 5 ribosomes, and 6 or more ribosomes were pooled, respectively, and are referred to hereafter as the Mono, Light and Heavy groups.

UTR library constituents were then reverse-transcribed and PCR-amplified from the three groups of RNA samples, before undergoing next-generation sequencing. To evaluate the effects of disease-associated variants on the distribution of corresponding transcripts across the Mono, Light and Heavy groups, we fit a negative binomial generalized linear model to read count for each UTR pair (wildtype/WT and mutant/mut) in three fraction groups while accounting for batch effects of the three experimental replicates (see Methods). The model primarily focused on discerning the distribution pattern of reads in three polysome fractions between UTR pairs, without considering differences in the expression levels of the UTR species. As a result, the analysis was unaffected by any perturbation of UTR sequence at the transcriptional level and did not account for changes in stoichiometry between UTRs and regulatory factors due to variations in expression levels. Consequently, we identified 483 high-confidence UTR pairs, comprising 396 pairs that did not alter translation (172 and 224 for 5' UTRs and 3' UTRs, respectively; collectively denoted by high-confidence nonsignificant or 'HC-nonsig' UTR variants), and 19 5' UTR and 27 3' UTR variants that significantly affected polysome distribution **(Fig. 2B, Supplemental Figs. S1, S2 and Table S2**; collectively denoted by high-confidence significant or 'HC-sig' UTR variants**)**. Pearson correlation analysis revealed R coefficients ranging from 0.59 to 0.71 for the mut-to-WT transcript ratios across three independent experiments **(Supplemental Fig. 3)**.

Although a very small proportion of UTR variants are categorized as pathogenic, we observed that HC-sig variants are enriched with known pathogenic variants relative to the HC-nonsig variants

(Fig. 2C), suggesting a contribution of translation-altering UTR variants to pathogenicity. Notably, we found that these translation-altering UTR variants are particularly prevalent in neurological and developmental disorders **(Supplemental Table S3)**.

Even with the high confidence dataset, we did not intend to immediately translate the altered polysome profile into an increase or decrease in translation efficiency, as the direction of the shift was not readily evident. Additionally, sedimentation in the sucrose gradient may have been partially affected by heavy particles other than ribosomes. Subsequently, individual reporters were used to examine the variants' effect on translation.

Validating the translation defects of mutant UTRs by luciferase reporter assay

The variants significantly altering the polysome profile were then individually validated through high-sensitivity luciferase reporter assays **(Fig. 3A)**. To this end, we resynthesized both the variant and corresponding wildtype alleles in the same library format - 115-nt native UTR segments centered on the variant and flanked by 20-nt priming sites. These UTRs were then cloned upstream (5') or downstream (3') of the firefly luciferase coding sequence, depending on their genomic location. As the initial library design, the test UTR segment differs only by one nucleotide, while a shared short UTR fragment is present on the opposite end of the coding sequence to ensure consistency across constructs **(Fig. 2A)**. To compare translation activity between wildtype and mutant UTRs, two reporter constructs of the same pair were transfected into independent wells of HEK293T cells, whereby their bioluminescence intensity was determined separately. Notably, to calibrate transfection efficiency across wells, the UTR reporter constructs were co-transfected with *Renilla* luciferase vector, and the firefly bioluminescence signal intensity was normalized to that of *Renilla*. Moreover, to control for potential variations in transcriptional activity, the relative firefly luminescence (mut/WT) of each UTR pair was further normalized to their cognate relative RNA level (mut/WT) (see Method). Our results indicate that 11 of the 12 selected HC-sig variants displayed prominent effects on translation activity **(Fig. 3A)**. Additionally, most of the tested UTR variants only altered translation efficiency but not RNA level, except for RFAXP:c.-101T>G **(Supplemental Fig. S3)**. Furthermore, we observed that 5' UTR variants had a greater impact on translation activity relative to 3' UTR variants **(Fig. 3C)**.

After validating individually the variants identified in our polysome profiling assay, we proceeded to investigate their effects on translation within an endogenous genomic context, targeting a total of eight variants (five in 5' UTRs and three in 3' UTRs). We derived the respective full-length UTR sequences from HEK293T cells and introduced the variants into cognate UTR amplicons via site-directed mutagenesis. Next, the UTR fragments were cloned into firefly luciferase reporter plasmids, which were then used for luciferase assay. 15 hours post transfection, the translation efficiency of the full-length UTR constructs was determined and normalized as described above. Despite being embedded in a longer genomic context, 7 of the 8 selected variants still significantly altered the translation activity of the full-length UTR constructs **(Fig. 3B)**. Moreover, we observed only minor variation in the mRNA levels of the luciferase reporter across the full-length UTR constructs, indicating that the observed phenotypes could not be attributed to discrepancies in transcriptional activity or RNA stability **(Supplemental Fig. S4)**. Furthermore, UTR variant-elicited regulation was highly consistent between full-length and short-form UTRs **(Fig. 3C)**, though the fold-change (mut/WT) in translation activity observed for full-length UTRs was much lower than for short-form UTRs, potentially due to the existence of additional regulatory elements in genomic milieus, which hindered or mitigated the impact of variants. Thus, our luciferase reporter assays

verify the robustness of our massively parallel polysome assay results. The disparity between full-length and short-form UTRs also highlights the strength and weakness of our strategy.

Polysome-shifting UTR variants promote motif gain/loss

We hypothesized that polysome-shifting UTR variants may result in the removal or gain of functional motifs that recruit *trans* factors responsible for regulating translation. Accordingly, we postulated that polysome-shifting variants would display distinct sequence properties. Therefore, first we investigated the nucleotide composition of polysome-shifting variants. We found that variations in C nucleotides (including gain and loss) in 5' UTRs were relatively inert in terms of translational alteration, whereas that was not the case for C in 3' UTRs **(Supplemental Fig. S5A and Table S4)**. Subsequently, we investigated the RBP-binding motifs of polysome-shifting UTR variants. Our results show that GAAGAA and T-rich motifs are enriched in HC-sig 5' UTRs, whereas G-rich and YTTC motifs are enriched in HC-sig 3' UTRs **(Supplemental Fig. S5B and Table S4,** Y represents T or C**)**. Furthermore, recognizing the intricate relationships between binding motifs and their corresponding RBPs, we conducted an additional analysis focusing on the RBPs themselves. This analysis suggested that TRA2B and members of the HNRNP family can bind HC-sig UTRs to regulate their translation **(Supplemental Fig. S5C)**. Extending this analysis, we calculated if changes in RBP-binding motifs are associated with changes in polysome profiles, which revealed that changes of SRSF1/2-, PABPN1- (AGAAG motifs) and CELF2- (T-rich motifs) binding sites in 5' UTRs frequently caused polysome shifting, so did mutations of binding sites for KHSRP (AGGG motifs) in 3' UTRs **(Fig. 4A)**.

To further validate the RBP-binding motifs identified by our enrichment analysis, we examined the effect of selected motifs on reporter expression by inserting them into a segment of the *MUTYH* 5' UTR or *MEFV* 3' UTR that contains suitable cloning sites (see Methods) and then perturbing its effect by mutating it so that it retained the same length but rendered it non-RBP-binding according to the ATtRACT RBP motif database (Giudice et al., 2016). For 5' UTR, GTTTTG and GAAGAAG motifs were selected for the test. Both selected motifs significantly increased the translation efficiency of luciferase reporters without affecting RNA expression level **(Fig. 4B)**. For 3' UTR CTTTTC and AGGGGGA motifs were selected for the test, yet neither of them significantly altered reporter expression. However, mutation of the AGGGGGA motif into AGCTGTA significantly reduced translation efficiency, indicative of a context-dependent effect of RBP-binding motifs **(Fig. 4C)**. This observation is consistent with additional findings where variants that create or disrupt specific RBP binding sites—such as SRSF1/2 **(**e.g., in *DMD* and *NF1*; **Fig. 3 and Supplemental Fig. S4)** and KHSRP **(**e.g., in *AL049650.1*; **Fig. 3 and Supplemental Figs. S4 & S5)**—led to significant changes in translation efficiency within their native UTR contexts.

Additionally, to assess the impact of RBPs on translation regulation through the short repeat sequence, we conducted a knockdown of SRSF2 using shRNA. This RBP was chosen due to its cytoplasmic localization (Thul et al., 2017) and abundant expression in HEK293T cells compared to other candidate RBPs. The results revealed that depleting SRSF2 eliminated the translation enhancement mediated by GAAGAAG, while having no effect on a non-SRSF2-binding motif **(Fig. 4D)**. While SRSF2 has not been direcr1tly implicated in translation regulation, some members of the SRSF family have been reported to function as translation regulators (Sliskovic et al., 2022). Notably, a mutation in the *NUMA1* 5' UTR that disrupted SRSF9 binding was previously demonstrated to decrease translation efficiency (Lim et al., 2021), providing further support for the involvement of SRSF family proteins in translation regulation. Together, these results support

the existence of mutational hotspots on short repeated sequences for polysome-shifting UTR variants and a collaborative regulatory effect of binding motifs.

Polysome-shifting mutations alter RNA secondary structure

Given that RNA secondary structure is believed to control translatability in addition to primary sequences (Georgakopoulos-Soares et al., 2022; Leppek et al., 2018), we determined the changes in folding energy elicited by sequence variations. To do so, we compared the folding energy change for variants in the HC-sig and HC-nonsig groups, which revealed that the 5' UTR HC-sig variants significantly weakened the folding structures and tended to prompt greater structural change than HC-nonsig variants, which was not the case for 3' UTR variants **(Fig. 5A)**. Furthermore, the HC-sig WT exhibited robust folding energy, potentially underlying their susceptibility of folding perturbations. In the same vein, RNA secondary structure predictions showed notable structural changes caused by 5' UTR single-nucleotide variations. As an example of the latter, we present the case of a 5' UTR single nucleotide variation in C-C chemokine receptor type 5 (CCR5) in Figure 5B. These results suggest that structural alterations of 5' UTRs by sequence variation could be a potential causal factor of the translation defects.

Since it has been shown previously that the usage of an uATG is affected by the surrounding UTR structure and can regulate translation of primary ORFs (Guenther et al., 2018; Xiang et al., 2023), we examined if the significant structural change elicited by HC-sig variants could be associated with the presence of uATG. Indeed, by contrasting UTR variants that did not alter uATG counts, we found that uATG-hosting UTRs were strongly associated with structural changes **(Fig. 5C)**. Therefore, while changes in uATG may not be common explanatory factors for polysome-shifting mutations, our results suggest that structure-modifying UTR variants may control primary ORF translation partly by interfering with translation initiation from a uORF.

Modeling the polysome-shifting UTR variants

Recognizing that polysome-shifting variants encompass diverse classes, such as those disrupting RBP binding or secondary structure, we employed statistical learning to discern the contributions of sequence and structural features to polysome shifting. Over 3,000 features, including evolutionary conservation, folding energy, secondary structures, RBP motifs, and k-mers, were collected. Features deemed insignificant or with an area under the receiver operating characteristic (AUROC) smaller than 0.5 by univariate logistic regression were filtered out (Methods). The remaining features were further refined using elastic net regression. Twelve features were selected to elucidate polysome-shifting variants in the 5' UTR, while eighteen were chosen for the 3' UTR **(Fig. 6A and Supplemental Table S5)**. Notably, GAA-repeat motifs of SRSF family binding sites again emerged as the most influential sequence feature for the 5' UTR. Additionally, changes in 'CAT' and 'AA' sequences, along with the folding energy of the 5' UTR, proved most effective in inducing polysome shifting. In contrast, for the 3' UTR, the structural contribution was less pronounced. Mutations altering GA- and T-rich sequences were identified as the strongest features promoting polysome shifting, consistent with prior analyses of RBP binding motifs **(Fig. 4)**. Model accuracy was validated against a test dataset not included in the training, with both the 5' UTR and 3' UTR models achieving an area under the receiver operating characteristic curve (AUROC) exceeding 0.8, underscoring the model's robustness **(Fig. 6B)**. To further assess generalizability, we applied the model to an external dataset that independently measured the effects of 5' UTR variants on polysome association (Sample et al., 2019). The model

achieved an AUROC of 0.75 on this external benchmark **(Fig. 6C)**, affirming its predictive power. Overall, our model supports the hypothesis that GA- and T-rich short repeat motifs serve as mutation hotspots for polysome-shifting mutations, while secondary structure exerts a greater influence on 5' UTR translation regulation compared to the 3' UTR.

The translation defect of a uORF-creating variant can be rescued by RNA editing

While uATG in the 5' UTR was not identified by the model as a widespread feature explaining polysome shifting, we hypothesize that it may still be a crucial factor. Its significance, however, might not have been universally captured across our library. Genome-wide analysis clearly indicated an enrichment of uORF disruption in the pathogenic UTR mutations **(Fig. 1B)**. Therefore, we aimed to dissect the regulatory mechanisms of uORFs underlying the effects of polysome-shifting variants and develop rescue strategies against pathogenic uORF mutations.

First, we examined whether the presence of uATG in general leads to lower translation in reporter assays. We observed that the presence of uATG in 5' UTRs of firefly luciferase was correlated with lower protein outputs **(Fig. 7A, Supplemental Table S6)**. Furthermore, two of the validated UTRs—Ferritin light chain (FTL) and Interferon Regulatory Factor 6 (IRF6)—demonstrated extreme translation perturbations **(Fig. 3)**. In a study by Luscieti et al., an FTL variant (c.-161C>T) was characterized as preventing 5' UTR stem-loop formation (Luscieti et al., 2013). As a consequence, the recruitment of suppressive iron regulatory proteins mediated by the 5' UTR stem-loop is disrupted, leading to an increase in translation activity. An IRF6 variant (c. -4609 G>A) was found previously to be associated with the developmental disorder Van der Woude syndrome (de Lima et al., 2009). The G>A variant was predicted to generate an out-of-frame uORF, but no experimental evidence has been provided yet. As shown in Figure 3, the corresponding full-length mutant UTR displayed a dramatic 9-fold reduction in translation efficiency, strongly indicating that presence of the uORF represses primary ORF translation. To verify the role of uATG, we performed western blotting to measure protein levels directly and determine protein size. To do so, we generated a third reporter construct that harbored the uORF in-frame to the coding region by deleting one nucleotide **(Fig. 7B)**. When probed with a luciferase-targeting antibody, the signal intensity for the out-of-frame mutant after normalization to the wildtype was only 0.089 **(Fig. 7C)**. This suggests that only a minute fraction of ribosomes may reinitiate at the canonical site or undergo leaky scanning at the uATG. Notably, the in-frame mutant, which represents a combination of the extended and the original forms, displayed a 0.24-fold signal intensity, indicating that uATG, despite lower initiation efficiency, markedly suppresses initiation at the canonical site. Compared to wildtype, we determined 0.6-fold translation efficiency, as measured by luciferase reporter assays, upon overexpression of the in-frame mutant **(Fig. 7D)** and no significant change in mRNA level was observed **(Supplemental Fig. S4)**. The discrepancy between protein abundance and luciferase intensity indicates that the extended form of the luciferase reporter may contribute to higher luminescence intensity.

To further validate the endogenous effect of the novel upstream ATG (uATG), we generated CRISPR knock-in clones carrying the IRF6:c.-4609G>A variant and examined its impact on gene expression. The introduction of the uATG reduced RNA levels to 88% and 37% of the wild-type in two independent clones **(Fig. 7E)**, and protein levels to 44% and 23%, respectively **(Fig. 7F)**, resulting in an overall reduction of translation efficiency to 50–62%. Although the uORF-mediated impairment of translation efficiency in IRF6 was clearly validated, we were unable to detect the corresponding micropeptide in the out-of-frame constructs (data not shown). It remains unclear

if micropeptides, if translated, play any role in pathogenesis. However, patients who have gained a uORF in the IRF6 5' UTR phenocopy Van der Woude patients hosting loss-of-function IRF6 mutations (de Lima et al., 2009).

Lastly, we aimed to develop rescue strategies that may be useful for future therapeutic purposes. We selected site-directed RNA editing using adenosine deaminase acting on RNA (ADAR) enzyme for this purpose to avoid genome editing and potential off-target effects. Upon binding of an antisense RNA to a target transcript, the ADAR enzyme catalyzes adenosine-to-inosine editing. Inosine is subsequently interpreted as guanosine during translation (Merkle et al., 2019; Qu et al., 2019). To achieve high editing efficiency, we overexpressed the antisense RNA coding construct and ADAR2 protein **(Fig. 7G)**. The transcribed antisense RNA encompasses a T>C mismatch that signals the complementary nucleotide for editing. First, we assessed editing efficiency by means of Sanger sequencing **(Fig. 7H)**. Only co-expression of antisense RNA and ADAR2 resulted in detectable editing, with an efficiency of ~21%. Luciferase signal intensities were also validated **(Fig. 7I)**. Consistently, expression of the antisense RNA alone had a very limited effect, but co-introduction of ADAR2 significantly increased the protein expression to ~50% the level of wildtype. Our promising results advocate the potential of clinical use of guided ADAR-RNA editing to reverse uORF-mediated translation suppression and thus alleviate the impact of the disease.

DISCUSSION

In this study, we applied massively parallel polysome assays to examine the effect of mutations in 5' and 3' UTRs in terms of RNA translatability **(Fig. 2)**. Our results show that the effect we observed in our high-throughput profiling is reliable, though it could be diluted somewhat in a more complex genomic context **(Fig. 3)**. We have shown that T- and GAA- repeat motifs are sensitive to translation-altering mutations **(Fig. 4)**, underscoring the involvement of both *cis*-regulatory sequences and *trans*-acting RBPs in regulating RNA translatability. Additionally, we identified the secondary structure of 5' UTRs as a critical factor controlling RNA translatability **(Fig. 5)**. We observed that alterations in folding energy, especially in uORF-hosting 5' UTRs, can have detrimental effects, suggesting structure-mediated uORF translation. These findings were summarized by elastic net regression models and robustly explained the polysome-shifting UTR variants **(Fig. 6)**. Additionally, the creation of uORFs in 5' UTRs through mutation adversely impacts primary ORF expression **(Fig. 7B-F)**, consistent with our finding of pathogenic mutant hotspot at uORF translation start sites **(Fig. 1B)**. We also reveal that ADAR-mediated editing can be deployed to rescue primary ORF translation **(Fig. 7G-I)**. Our study emphasizes the significant role of precise UTR translation regulation in gene expression and offers a molecular explanation for the impact of UTR mutations on pathogenicity. Below, we discuss some of the strengths and limitations of our study.

Massively parallel evaluation of translation efficiency

Translation efficiency is a key post-transcriptional regulation to control gene output. Efforts have been made to assess translation efficiency systematically in terms of gene structures and sequences (Jia et al., 2020; Leppek et al., 2022; Niederer et al., 2022; Oikonomou et al., 2014; Sample et al., 2019; Savinov et al., 2021; Slutskin et al., 2018; Wissink et al., 2016; Zhao et al., 2014). One way to measure translation efficiency is according to protein output. For instance, in MPRA where reporter sequences are fixed and fused with test sequences, the expression of the reporter fluorescent proteins is determined by Fluorescence Activated Cell Sorting (FACS), with

expression being normalized to the level of the other fluorescent reporter from the same construct to account for experimental bias. The tested sequences within each bin are then determined by sequencing. Mass spectrometry can be employed to determine quantitatively endogenous protein levels (Baek et al., 2008). Although this method is relatively quantitative, MPRA has the leverage over RNA stability, especially if the reporter is fused with various UTRs. Moreover, the results for endogenous proteins are influenced by protein turnover, which itself is a very important means of controlling gene expression. Thus, although protein output is a crucial readout of gene expression, this approach does not provide a direct measurement of translation efficiency.

The alternative method to measure translation is through polysome profiling. For endogenous genes, ribosome footprinting can be employed to quantify transcript fragments associated with ribosomes. For MPRA, in which the coding footprint is identical for the whole library, polysome profiling is used instead. Rather than sequencing and then counting transcript fragments attached to ribosomes, polysome profiling does not shear off the transcript, but only fractionates RNAs according to the number (size) of associated ribosomes through ultracentrifugation in a sucrose gradient, representing the most direct way to measure the efficiency of RNAs to recruit ribosomes. However, there are some limitations to this method. First, there is considerable variation in how polysome fractions are used. Some studies have used the average number of ribosomes on each reporter, with each fraction (including the 'ribosome-free' fraction) being considered and the average ribosome number being calculated according to the relative distribution of the transcript in polysomes . In contrast, others use only some of the fractions to infer translation efficiency. For example, percentage translated RNAs in polysomes can be used to infer ribosome loading (Jia et al., 2020; Schuster et al., 2023), and the monosome to input ratio (recruitment score) can be calculated to infer ribosome recruitment efficiency (Niederer et al., 2022). These alternative approaches to analyzing the data create perplexity to interpret polysome profiles. Another major limitation of polysome profiling is its dependency on promoters. It has been reported that whether polysome profiles reflect translation efficiency is contingent on the promoters driving gene expression (Kong et al., 2008). It remains unclear if the strong expression promoters (such as the CMV promoter) commonly used for MPRA are optimal for revealing differences in polysome profiles. Moreover, because not all ribosomes translate actively on transcripts, they can be slowed, stalled, or collided on a transcript (Meydan & Guydosh, 2021). Although it has been proposed that the major bottleneck of the translation reaction is translation initiation, elongation also contributes to translation efficiency (Riba et al., 2019). Thus, whether the number of ribosomes associated with a transcript truly reflects translation efficiency, especially for endogenous transcripts in diverse coding contexts, remains elusive.

Severe translation defects caused by 5' UTR point mutations

The 5' UTR serves as the major ribosome entry site for translation. In our data, we observed remarkable changes in translation efficiency elicited by 5' UTR point mutations **(Fig. 3)**, with IRF6:c.-4609G>A and FTL:c.-161C>T protein outputs being reduced 10-30-fold without affecting respective RNA levels **(Supplemental Figs. S3, S4)**. The impacts of 3' UTR mutations appear to be more additive and context-dependent, consistent with its nature of greater length variation. The most severe UTR mutation we identified in our MPRA dataset is IRF6:c.-4609G>A, which has been observed in Van der Woude syndrome patients. This 5' UTR mutation has been suggested to suppress IRF6 translation by generating a uORF. We have demonstrated herein that IRF6:c.-4609G>A creates a strong upstream translation start codon, dramatically reducing protein output

from the primary ORF **(Fig. 7B-F)**. We reasoned that a G>A mutation represented an optimal target for ADAR editing, allowing us to switch A back to I, which is read as G by the cellular machinery **(Fig. 7G-I)**. Another advantage of ADAR is that editing operates at the RNA level within the potential treatment window, thereby restoring desired protein function without causing any permanent alterations to the DNA.

Ferritin is composed of L (FTL) and H (FTH) subunits, and it is responsible for regulating the storage and intracellular distribution of iron. FTL:c.-161C, one of the UTR variants we observed as eliciting strongly perturbed translation, has been mapped as part of a noncanonical upstream start codon (CAG, TISdb) (Wan & Qian, 2014). It is likely that the C>T mutation disrupts uORF initiation, thereby releasing repression of the primary ORF, and promoting the ~10-fold increase in translation. However, the 5' UTR of FTL is also responsible for forming an IRE stem-loop (Klausner et al., 1993). The FTL:c.-161C>T mutation likely disrupts this hexanucleotide loop structure, preventing it from interacting with the Iron Regulatory Proteins IRP1 and IRP2 (Luscieti et al., 2013). Since IRPs bind to IREs under iron-deficient conditions to suppress translation of both ferritin subunits (Muckenthaler et al., 1998), mutations that abolish IRP-IRE interactions elicit aberrant production of ferritins and are the major causative mutations of Hereditary Hyperferritinaemia Cataract Syndrome. Thus, our massively parallel polysome profiling has uncovered known and novel mutations that cause translation defects, serving as a genetic diagnostic tool for identifying crucial and clinically relevant regulatory mutations.

DATA AVAILABILITY

All raw and processed sequencing data generated in this study have been submitted to the NCBI Gene Expression Omnibus (GEO; https://www.ncbi.nlm.nih.gov/geo/) under accession number GSE229492 (reviewer token oxcpuuechhihzuf).

Codes used for the analyses in this study have been deposited at https://github.com/chienlinglin/modeling-UTR-variants-polysome/

Other databases used in the study:

AREsite2: http://nibiru.tbi.univie.ac.at/AREsite2

ATtRACT: https://attract.cnic.es/download

FUNDING

This work was supported by a Career Development Award and the Multidisciplinary Health Cloud Research Program of Academia Sinica (AS-CDA-108-M03 and AS-PH-109-01-3), a Career Development Award from the National Health Research Institutes, Taiwan (NHRI-EX112-10908BC), and Excellent Young Scholar Research Grants and a Ta-You Wu Memorial Award from the National Science and Technology Council, Taiwan (NSTC 112-2628-B-001-009, MOST 111-2628-B-001-003 and 108-2118-M-001-013-MY5). H-L C is supported by NSTC Postdoc Fellowship (NSTC 112-2811-B-001-035).

ACKNOWLEDGEMENTS

We thank the Genomics Core and the Bioinformatics Core of the Institute of Molecular Biology (IMB), Academia Sinica, for performing the amplicon sequencing and for providing computing resources. We thank all members of IMB for tremendous help and support.

COMPETING INTEREST STATEMENT

The authors declare no competing interests.

AUTHOR CONTRIBUTIONS

C-L L and H-L C designed the experiments. W-P L established the MPRA. Y-L W and J-Y S carried out modeling and analyses. W-P L, Y-C C, H-L C, Y-H C, Y-L K, B-J C, Y-T Hsieh and C-H Y performed experiments. Y-T Huang supervised the statistical analysis. W-P L, Y-C C, Y-L W and C-L L wrote the manuscript.

REFERENCES

Abell, N. S., DeGorter, M. K., Gloudemans, M. J., Greenwald, E., Smith, K. S., He, Z. H., & Montgomery, S. B. (2022). Multiple causal variants underlie genetic associations in humans. *Science*, *375*(6586), 1247-+. https://doi.org/10.1126/science.abj5117

Agarwal, V., Bell, G. W., Nam, J. W., & Bartel, D. P. (2015). Predicting effective microRNA target sites in mammalian mRNAs. *Elife*, *4*. https://doi.org/ARTNe05005
10.7554/eLife.05005

Baek, D., Villén, J., Shin, C., Camargo, F. D., Gygi, S. P., & Bartel, D. P. (2008). The impact of microRNAs on protein output. *Nature*, *455*(7209), 64-U38. https://doi.org/10.1038/nature07242

Barreau, C., Paillard, L., & Osborne, H. B. (2005). AU-rich elements and associated factors: are there unifying principles? *Nucleic Acids Research*, *33*(22), 7138-7150. https://doi.org/10.1093/nar/gki1012

Beffagna, G., Occhi, G., Nava, A., Vitiello, L., Ditadi, A., Basso, C., Bauce, B., Carraro, G., Thiene, G., Towbin, J. A., Danieli, G. A., & Rampazzo, A. (2005). Regulatory mutations in transforming growth factor-β3 gene cause arrhythmogenic right ventricular cardiomyopathy type 1. *Cardiovascular Research*, *65*(2), 366-373. https://doi.org/10.1016/j.cardiores.2004.10.005

Bolger, A. M., Lohse, M., & Usadel, B. (2014). Trimmomatic: a flexible trimmer for Illumina sequence data. *Bioinformatics*, *30*(15), 2114-2120. https://doi.org/10.1093/bioinformatics/btu170

Chiang, H.-L., Chen, Y.-T., Su, J.-Y., Lin, H.-N., Yu, C.-H. A., Hung, Y.-J., Wang, Y.-L., Huang, Y.-T., & Lin, C.-L. (2022). Mechanism and modeling of human disease-associated near-exon intronic variants that perturb RNA splicing. *Nature Structural & Molecular Biology*. https://doi.org/10.1038/s41594-022-00844-1

Choe, J., Lin, S. B., Zhang, W. C., Liu, Q., Wang, L. F., Ramirez-Moya, J., Du, P., Kim, W., Tang, S. J., Sliz, P., Santisteban, P., George, R. E., Richards, W. G., Wong, K. K., Locker, N., Slack, F. J., & Gregory, R. I. (2018). mRNA circularization by METTL3-eIF3h enhances translation and promotes oncogenesis. *Nature*, *561*(7724), 556-+. https://doi.org/10.1038/s41586-018-0538-8

Danecek, P., Bonfield, J. K., Liddle, J., Marshall, J., Ohan, V., Pollard, M. O., Whitwham, A., Keane, T., McCarthy, S. A., Davies, R. M., & Li, H. (2021). Twelve years of SAMtools and BCFtools. *Gigascience*, *10*(2). https://doi.org/ARTN giab008
10.1093/gigascience/giab008

de Lima, R. L. L. F., Hoper, S. A., Ghassibe, M., Cooper, M. E., Rorick, N. K., Kondo, S., Katz, L., Marazita, M. L., Compton, J., Bale, S., Hehr, U., Dixon, M. J., Daack-Hirsch, S., Boute, O., Bayet, B., Revencu, N., Verellen-Dumoulin, C., Vikkula, M., Richieri-Costa, A., . . . Schutte, B. C. (2009). Prevalence and nonrandom distribution of exonic mutations in interferon regulatory factor 6 in 307 families with Van der Woude syndrome and 37 families with popliteal pterygium syndrome. *Genetics in Medicine*, *11*(4), 241-247. https://doi.org/10.1097/GIM.0b013e318197a49a

Dusl, M., Senderek, J., Müller, J. S., Vogel, J. G., Pertl, A., Stucka, R., Lochmüller, H., David, R., & Abicht, A. (2015). A 3'-UTR mutation creates a microRNA target site in the
gene of patients with congenital myasthenic syndrome. *Human Molecular Genetics*, *24*(12), 3418-3426. https://doi.org/10.1093/hmg/ddv090

Fay, M. M., Lyons, S. M., & Ivanov, P. (2017). RNA G-Quadruplexes in Biology: Principles and Molecular Mechanisms. *Journal of Molecular Biology*, *429*(14), 2127-2147. https://doi.org/10.1016/j.jmb.2017.05.017

Gandin, V., Sikstrom, K., Alain, T., Morita, M., McLaughlan, S., Larsson, O., & Topisirovic, I. (2014). Polysome fractionation and analysis of mammalian translatomes on a genome-wide scale. *J Vis Exp*(87). https://doi.org/10.3791/51455

Georgakopoulos-Soares, I., Parada, G. E., & Hemberg, M. (2022). Secondary structures in RNA synthesis, splicing and translation. *Computational and Structural Biotechnology Journal*, *20*, 2871-2884. https://doi.org/10.1016/j.csbj.2022.05.041

Giudice, G., Sanchez-Cabo, F., Torroja, C., & Lara-Pezzi, E. (2016). ATtRACT-a database of RNA-binding proteins and associated motifs. *Database-the Journal of Biological Databases and Curation*. https://doi.org/ARTN baw035
10.1093/database/baw035

Griesemer, D., Xue, J. R., Reilly, S. K., Ulirsch, J. C., Kukreja, K., Davis, J. R., Kanai, M., Yang, D. K., Butts, J. C., Guney, M. H., Luban, J., Montgomery, S. B., Finucane, H. K., Novina, C. D., Tewhey, R., & Sabeti, P. C. (2021). Genome-wide functional screen of 3 ' UTR variants uncovers causal variants for human disease and evolution. *Cell*, *184*(20), 5247-+. https://doi.org/10.1016/j.cell.2021.08.025

Guenther, U. P., Weinberg, D. E., Zubradt, M. M., Tedeschi, F. A., Stawicki, B. N., Zagore, L. L., Brar, G. A., Licatalosi, D. D., Bartel, D. P., Weissman, J. S., & Jankowsky, E. (2018). The helicase Ded1p controls use of near-cognate translation initiation codons in 5´ UTRs. *Nature*, *559*(7712), 130-+. https://doi.org/10.1038/s41586-018-0258-0

Jia, L. F., Mao, Y. H., Ji, Q. Q., Dersh, D., Yewdell, J. W., & Qian, S. B. (2020). Decoding mRNA translatability and stability from the 5 ' UTR. *Nature Structural & Molecular Biology*, *27*(9), 814-+. https://doi.org/10.1038/s41594-020-0465-x

Kerpedjiev, P., Hammer, S., & Hofacker, I. L. (2015). Forna (force-directed RNA): Simple and effective online RNA secondary structure diagrams. *Bioinformatics*, *31*(20), 3374-3376. https://doi.org/10.1093/bioinformatics/btv372

Klausner, R. D., Rouault, T. A., & Harford, J. B. (1993). Regulating the Fate of Messenger-Rna - the Control of Cellular Iron-Metabolism. *Cell*, *72*(1), 19-28. https://doi.org/Doi 10.1016/0092-8674(93)90046-S

Komar, A. A., & Hatzoglou, M. (2005). Internal ribosome entry sites in cellular mRNAs: Mystery of their existence. *Journal of Biological Chemistry*, *280*(25), 23425-23428. https://doi.org/10.1074/jbc.R400041200

Kong, Y. W., Cannell, I. G., de Moor, C. H., Hill, K., Garside, P. G., Hamilton, T. L., Meijer, H. A., Dobbyn, H. C., Stoneley, M., Spriggs, K. A., Willis, A. E., & Bushell, M. (2008). The mechanism of micro-RNA-mediated translation repression is determined by the promoter of the target gene. *Proceedings of the National Academy of Sciences of the United States of America*, *105*(26), 8866-8871. https://doi.org/10.1073/pnas.0800650105

Kuhn, M. (2008). Building Predictive Models in R Using the caret Package. *Journal of Statistical Software*, *28*(5), 1-26. https://doi.org/DOI 10.18637/jss.v028.i05

Kumari, S., Bugaut, A., Huppert, J. L., & Balasubramanian, S. (2007). An RNA G-quadruplex in the 5´ UTR of the NRAS proto-oncogene modulates translation. *Nature Chemical Biology*, *3*(4), 218-221. https://doi.org/10.1038/nchembio864

Landrum, M. J., Lee, J. M., Benson, M., Brown, G., Chao, C., Chitipiralla, S., Gu, B., Hart, J., Hoffman, D., Hoover, J., Jang, W., Katz, K., Ovetsky, M., Riley, G., Sethi, A., Tully, R., Villamarin-Salomon, R., Rubinstein, W., & Maglott, D. R. (2016). ClinVar: public archive of interpretations of clinically relevant variants. *Nucleic Acids Research*, *44*(D1), D862-D868. https://doi.org/10.1093/nar/gkv1222

Leppek, K., Byeon, G. W., Kladwang, W., Wayment-Steele, H. K., Kerr, C. H., Xu, A. D. F., Kim, D., Topkar, V. V., Choe, C., Rothschild, D., Tiu, G. C., Wellington-Oguri, R., Fujii, K., Sharma, E., Watkins, A. M., Nicol, J. J., Romano, J., Tunguz, B., Diaz, F., . . . Das, R. (2022). Combinatorial optimization of mRNA structure, stability, and translation for RNA-based therapeutics. *Nature Communications*, *13*(1). https://doi.org/ARTN 1536
10.1038/s41467-022-28776-w

Leppek, K., Das, R., & Barna, M. (2018). Functional 5 ' UTR mRNA structures in eukaryotic translation regulation and how to find them (vol 19, pg 158, 2018). *Nature Reviews Molecular Cell Biology*, *19*(10), 673-673. https://doi.org/10.1038/s41580-018-0055-5

Lim, Y. T., Arora, S., Schuster, S. L., Corey, L., Fitzgibbon, M., Wladyka, C. L., Wu, X. Y., Coleman, I. M., Delrow, J. J., Corey, E., True, L. D., Nelson, P. S., Ha, G., & Hsieh, A. C. (2021). Multiplexed functional genomic analysis of 5' untranslated region mutations across the spectrum of prostate cancer. *Nature Communications*, *12*(1). https://doi.org/ARTN 4217
10.1038/s41467-021-24445-6

Litterman, A. J., Kageyama, R., Le Tonqueze, O., Zhao, W. X., Gagnon, J. D., Goodarzi, H., Erle, D. J., & Ansel, K. M. (2019). A massively parallel 3 ' UTR reporter assay reveals relationships between nucleotide content, sequence conservation, and mRNA destabilization. *Genome Research*, *29*(6), 896-906. https://doi.org/10.1101/gr.242552.118

Lorenz, R., Bernhart, S. H., Siederdissen, C. H. Z., Tafer, H., Flamm, C., Stadler, P. F., & Hofacker, I. L. (2011). ViennaRNA Package 2.0. *Algorithms for Molecular Biology*,

6. https://doi.org/Artn 26
10.1186/1748-7188-6-26
Luscieti, S., Tolle, G., Aranda, J., Benet-Campos, C., Risse, F., Moran, E., Muckenthaler, M. U., & Sanchez, M. (2013). Novel Mutations in the Ferritin-L Iron-Responsive Element That Only Mildly Impair Irp Binding Cause Hereditary Hyperferritinaemia Cataract Syndrome. *American Journal of Hematology*, *88*(5), E63-E63. <Go to ISI>://WOS:000318043500099
MacArthur, J., Bowler, E., Cerezo, M., Gil, L., Hall, P., Hastings, E., Junkins, H., McMahon, A., Milano, A., Morales, J., Pendlington, Z. M., Welter, D., Burdett, T., Hindorff, L., Flicek, P., Cunningham, F., & Parkinson, H. (2017). The new NHGRI-EBI Catalog of published genome-wide association studies (GWAS Catalog). *Nucleic Acids Research*, *45*(D1), D896-D901. https://doi.org/10.1093/nar/gkw1133
Mayya, V. K., & Duchaine, T. F. (2019). Ciphers and Executioners: How 3 '-Untranslated Regions Determine the Fate of Messenger RNAs. *Frontiers in Genetics*, *10*. https://doi.org/ARTN 6
10.3389/fgene.2019.00006
Mazumder, B., Seshadri, V., & Fox, P. L. (2003). Translational control by the 3 ´ -UTR:: the ends specify the means. *Trends in Biochemical Sciences*, *28*(2), 91-98. https://doi.org/10.1016/S0968-0004(03)00002-1
Merkle, T., Merz, S., Reautschnig, P., Blaha, A., Li, Q., Vogel, P., Wettengel, J., Li, J. B., & Stafforst, T. (2019). Precise RNA editing by recruiting endogenous ADARs with antisense oligonucleotides. *Nature Biotechnology*, *37*(2), 133-+. https://doi.org/10.1038/s41587-019-0013-6
Meydan, S., & Guydosh, N. R. (2021). A cellular handbook for collided ribosomes: surveillance pathways and collision types. *Current Genetics*, *67*(1), 19-26. https://doi.org/10.1007/s00294-020-01111-w
Mikl, M., Eletto, D., Nijim, M., Lee, M., Lafzi, A., Mhamedi, F., David, O., Sain, S. B., Handler, K., & Moor, A. E. (2022). A massively parallel reporter assay reveals focused and broadly encoded RNA localization signals in neurons. *Nucleic Acids Research*, *50*(18), 10643-10664. https://doi.org/10.1093/nar/gkac806
Muckenthaler, M., Gray, N. K., & Hentze, M. W. (1998). IRP-1 binding to ferritin mRNA prevents the recruitment of the small ribosomal subunit by the cap-binding complex elF4F. *Molecular Cell*, *2*(3), 383-388. https://doi.org/Doi 10.1016/S1097-2765(00)80282-8
Niederer, R. O., Rojas-Duran, M. F., Zinshteyn, B., & Gilbert, W. V. (2022). Direct analysis of ribosome targeting illuminates thousand-fold regulation of translation initiation. *Cell Systems*, *13*(3), 256-+. https://doi.org/10.1016/j.cels.2021.12.002
Oikonomou, P., Goodarzi, H., & Tavazoie, S. (2014). Systematic Identification of Regulatory Elements in Conserved 3 ' UTRs of Human Transcripts. *Cell Reports*, *7*(1), 281-292. https://doi.org/10.1016/j.celrep.2014.03.001
Pagès H, A. P., Gentleman R, DebRoy S. (2022). *Biostrings: Efficient manipulation of biological strings. R package version 2.66.0*. https://bioconductor.org/packages/Biostrings
Qu, L., Yi, Z. Y., Zhu, S. Y., Wang, C. H., Cao, Z. Z., Zhou, Z., Yuan, P. F., Yu, Y., Tian, F., Liu, Z. H., Bao, Y., Zhao, Y. X., & Wei, W. S. (2019). Programmable RNA

editing by recruiting endogenous ADAR using engineered RNAs (vol 37, pg 1059, 2019). *Nature Biotechnology*, *37*(11), 1380-1380. https://doi.org/10.1038/s41587-019-0292-y

Quinlan, A. R., & Hall, I. M. (2010). BEDTools: a flexible suite of utilities for comparing genomic features. *Bioinformatics*, *26*(6), 841-842. https://doi.org/10.1093/bioinformatics/btq033

R-Core-Team. (2021). *R: A Language and Environment for Statistical Computing. R Foundation for Statistical Computing, Vienna.* https://www.R-project.org

Rabani, M., Pieper, L., Chew, G. L., & Schier, A. F. (2017). A Massively Parallel Reporter Assay of 3 ' UTR Sequences Identifies In Vivo Rules for mRNA Degradation. *Molecular Cell*, *68*(6), 1083-+. https://doi.org/10.1016/j.molcel.2017.11.014

Riba, A., Di Nanni, N., Mittal, N., Arhné, E., Schmidt, A., & Zavolan, M. (2019). Protein synthesis rates and ribosome occupancies reveal determinants of translation elongation rates. *Proceedings of the National Academy of Sciences of the United States of America*, *116*(30), 15023-15032. https://doi.org/10.1073/pnas.1817299116

Saito, T., & Rehmsmeier, M. (2017). Precrec: fast and accurate precision-recall and ROC curve calculations in R. *Bioinformatics*, *33*(1), 145-147. https://doi.org/10.1093/bioinformatics/btw570

Sample, P. J., Wang, B., Reid, D. W., Presnyak, V., McFadyen, I. J., Morris, D. R., & Seelig, G. (2019). Human 5 ' UTR design and variant effect prediction from a massively parallel translation assay. *Nature Biotechnology*, *37*(7), 803-+. https://doi.org/10.1038/s41587-019-0164-5

Savinov, A., Brandsen, B. M., Angell, B. E., Cuperus, J. T., & Fields, S. (2021). Effects of sequence motifs in the yeast 3 ' untranslated region determined from massively parallel assays of random sequences. *Genome Biology*, *22*(1). https://doi.org/ARTN 293
10.1186/s13059-021-02509-6

Schuster, S. L., Arora, S., Wladyka, C. L., Itagi, P., Corey, L., Young, D., Stackhouse, B. L., Kollath, L., Wu, Q. V., Corey, E., True, L. D., Ha, G., Paddison, P. J., & Hsieh, A. C. (2023). Multi-level functional genomics reveals molecular and cellular oncogenicity of patient-based 3' untranslated region mutations. *Cell Reports*, *42*(8). https://doi.org/ARTN 112840
10.1016/j.celrep.2023.112840

Serikawa, T., Spanos, C., von Hacht, A., Budisa, N., Rappsilber, J., & Kurreck, J. (2018). Comprehensive identification of proteins binding to RNA G-quadruplex motifs in the 5 ´ UTR of tumor-associated mRNAs. *Biochimie*, *144*, 169-184. https://doi.org/10.1016/j.biochi.2017.11.003

Sherry, S. T., Ward, M. H., & Sirotkin, K. (1999). dbSNP - Database for single nucleotide polymorphisms and other classes of minor genetic variation. *Genome Research*, *9*(8), 677-679. <Go to ISI>://WOS:000082063000002

Sliskovic, I., Eich, H., & Muller-McNicoll, M. (2022). Exploring the multifunctionality of SR proteins. *Biochem Soc Trans*, *50*(1), 187-198. https://doi.org/10.1042/BST20210325

Slutskin, I. V., Weingarten-Gabbay, S., Nir, R., Weinberger, A., & Segal, E. (2018). Unraveling the determinants of microRNA mediated regulation using a massively

parallel reporter assay. *Nature Communications*, *9*. https://doi.org/ARTN 529
10.1038/s41467-018-02980-z

Smith, T., Heger, A., & Sudbery, I. (2017). UMI-tools: modeling sequencing errors in Unique Molecular Identifiers to improve quantification accuracy. *Genome Research*, *27*(3), 491-499. https://doi.org/10.1101/gr.209601.116

Stenson, P. D., Mort, M., Ball, E. V., Evans, K., Hayden, M., Heywood, S., Hussain, M., Phillips, A. D., & Cooper, D. N. (2017). The Human Gene Mutation Database: towards a comprehensive repository of inherited mutation data for medical research, genetic diagnosis and next-generation sequencing studies. *Human Genetics*, *136*(6), 665-677. https://doi.org/10.1007/s00439-017-1779-6

Steri, M., Idda, M. L., Whalen, M. B., & Orru, V. (2018). Genetic variants in mRNA untranslated regions. *Wiley Interdisciplinary Reviews-Rna*, *9*(4). https://doi.org/ARTN e1474
10.1002/wrna.1474

Stoecklin, G., Stoeckle, P., Lu, M., Muehlemann, O., & Moroni, C. (2001). Cellular mutants define a common mRNA degradation pathway targeting cytokine AU-rich elements. *Rna*, *7*(11), 1578-1588. <Go to ISI>://WOS:000172225800007

Thul, P. J., Åkesson, L., Wiking, M., Mahdessian, D., Geladaki, A., Blal, H. A., Alm, T., Asplund, A., Björk, L., Breckels, L. M., Bäckström, A., Danielsson, F., Fagerberg, L., Fall, J., Gatto, L., Gnann, C., Hober, S., Hjelmare, M., Johansson, F., . . . Lundberg, E. (2017). A subcellular map of the human proteome. *Science*, *356*(6340). https://doi.org/ARTN eaal3321
10.1126/science.aal3321

Van Etten, J., Schagat, T. L., Hrit, J., Weidmann, C. A., Brumbaugh, J., Coon, J. J., & Goldstrohm, A. C. (2012). Human Pumilio Proteins Recruit Multiple Deadenylases to Efficiently Repress Messenger RNAs. *Journal of Biological Chemistry*, *287*(43), 36370-36383. https://doi.org/10.1074/jbc.M112.373522

Wan, J., & Qian, S. B. (2014). TISdb: a database for alternative translation initiation in mammalian cells. *Nucleic Acids Research*, *42*(D1), D845-D850. https://doi.org/10.1093/nar/gkt1085

Wells, S. E., Hillner, P. E., Vale, R. D., & Sachs, A. B. (1998). Circularization of mRNA by eukaryotic translation initiation factors. *Molecular Cell*, *2*(1), 135-140. https://doi.org/Doi 10.1016/S1097-2765(00)80122-7

Wissink, E. M., Fogarty, E. A., & Grimson, A. (2016). High-throughput discovery of post-transcriptional cis-regulatory elements. *Bmc Genomics*, *17*. https://doi.org/ARTN 177
10.1186/s12864-016-2479-7

Xiang, Y. Z., Huang, W. Z., Tan, L. M., Chen, T. Y., He, Y., Irving, P. S., Weeks, K. M., Zhang, Q. C., & Dong, X. N. (2023). Pervasive downstream RNA hairpins dynamically dictate start-codon selection. *Nature*. https://doi.org/10.1038/s41586-023-06500

Zhao, W. X., Pollack, J. L., Blagev, D. P., Zaitlen, N., McManus, M. T., & Erle, D. J. (2014). Massively parallel functional annotation of 3 ' untranslated regions. *Nature Biotechnology*, *32*(4), 387-U259. https://doi.org/10.1038/nbt.2851

Figures

Figure 1

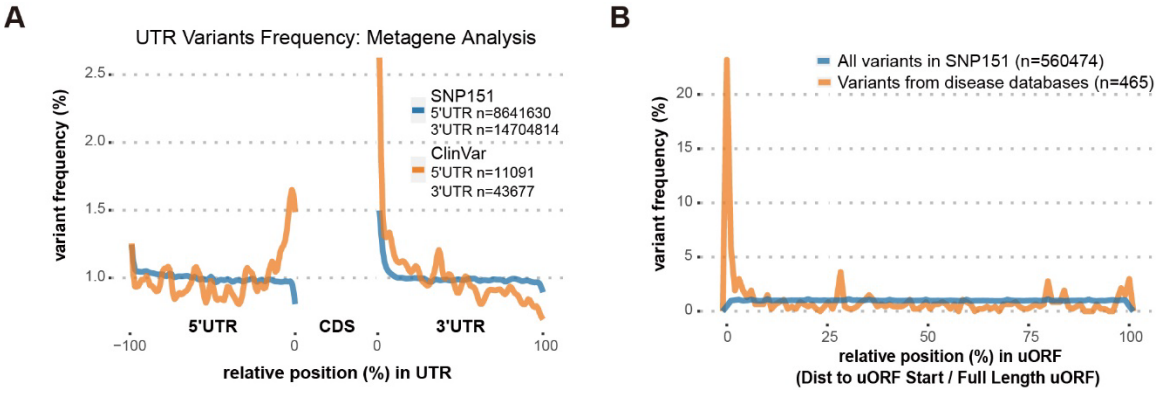

Figure 1. Enrichment of UTR variants relative to open reading frames. (A) Metagene analysis of native human UTRs (blue line) or disease-relevant variants reported in ClinVar (orange line). Note the enrichment of UTR variants near the coding region. **(B)** Metagene analysis of all native human variants (blue line) or disease-relevant variants reported in ClinVar and HGMD (orange line) in relation to uORFs. Note the distinct enrichment of disease-relevant variants at the uORF start site.

Figure 2

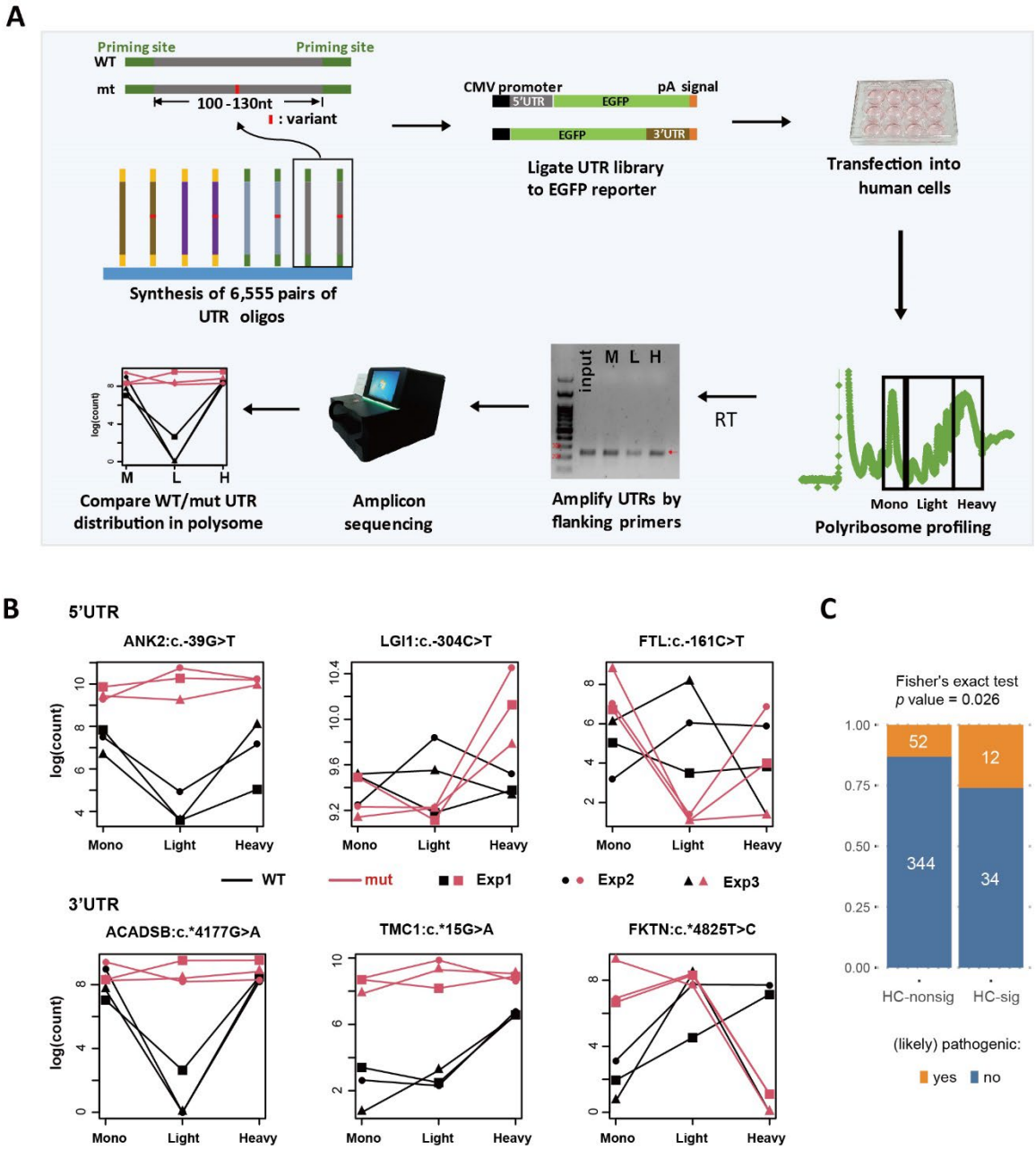

Figure 2. Massively parallel polysome assays. (A) UTR fragments were synthesized in bulk and ligated with EGFP reporters for expression in human cells. The reporter-expressing cell lysate was fractionated into monosome, light (2-5 ribosomes) and heavy (6+ ribosomes) polysome-containing fractions, and the UTR library was then amplified for amplicon sequencing. Mutations that altered relative distribution among fractions were defined as significant polysome-shifting mutations. **(B)** Examples of UTR pairs that significantly differed in polysome distribution. **(C)** Enrichment of pathogenic variants among HC-sig polysome-shifting UTR variants.

Figure 3

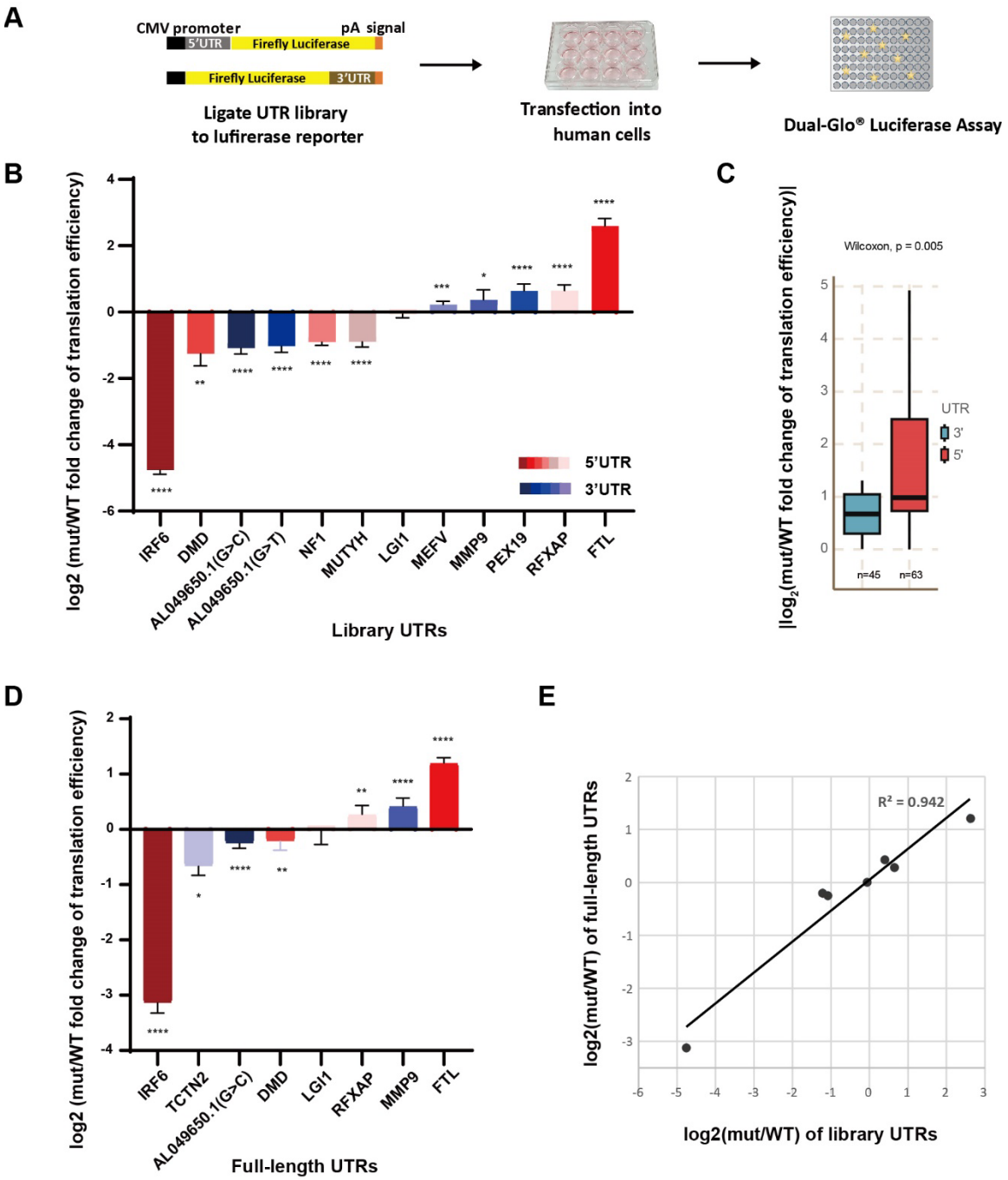

Figure 3. Validation of mutant effect on translation by luciferase assays. (A) Selected UTRs were ligated with firefly luciferase reporters and co-transfected with *Renilla* luciferase into human cells. The firefly luminescence was first normalized to the *Renilla* luminescence, and further normalized to the respective RNA expression levels to determine translation efficiency. The log2 value of mut over WT translation efficiency was plotted ascendingly. **(B)** Translation efficiency of eight full-length UTR pairs was examined in the same manner as in (A). UTR pairs are color-coded according to their gene origin (A&B). The individual assays were repeated three times and the differences

were accessed by a two-tailed Student t-test: *: $p < 0.05$, **: $p < 0.01$, ***: $p < 0.001$, ****: $p < 0.0001$ (A&B). **(C)** Absolute log2 translation efficiency changes (mut vs. WT) were compared between 5' and 3' UTR variants, as shown in (B). Statistical significance was assessed using a two-sided Wilcoxon rank-sum test. **(D)** Comparison of the effect of mutations on the translation efficiency of library (short) and full-length forms of UTRs.

Figure 4

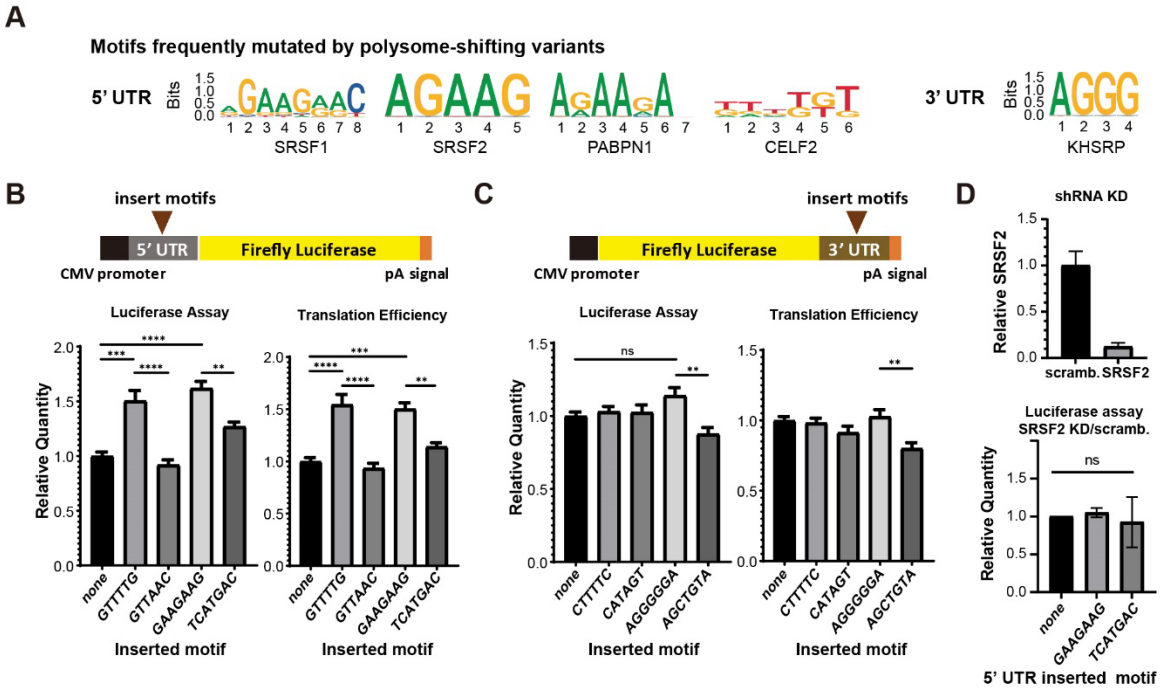

Figure 4. Identification of polysome-shifting RBP-binding motifs. (A) Motifs significantly more frequently mutated by HC-sig variants. **(B)** Two 5' UTR-enriched motifs from (A), i.e., GTTTTG and GAAGAAG, were inserted into a 5' UTR of firefly luciferase to determine their luciferase activity and normalized translation efficiency. Mutant forms of these two motifs, GTTAAC and TCATGAC, were generated for comparison. **(C)** Similar to the 5' UTR design in (B), the 3' UTR-enriched motifs CTTTTC and AGGGGGA were examined against their mutant forms, i.e., CATAGT and AGCTGTA. The individual assays were repeated four times. Statistical significance was determined by a two-tailed Student t-test: **: $p < 0.01$, ***: $p < 0.001$, ****: $p < 0.0001$. **(D)** Upper: Relative SRSF2 transcript levels, as determined by RT-qPCR. Lower: Relative luciferase activity with various 5' UTR motifs, normalized to scrambled shRNA infection.

Figure 5

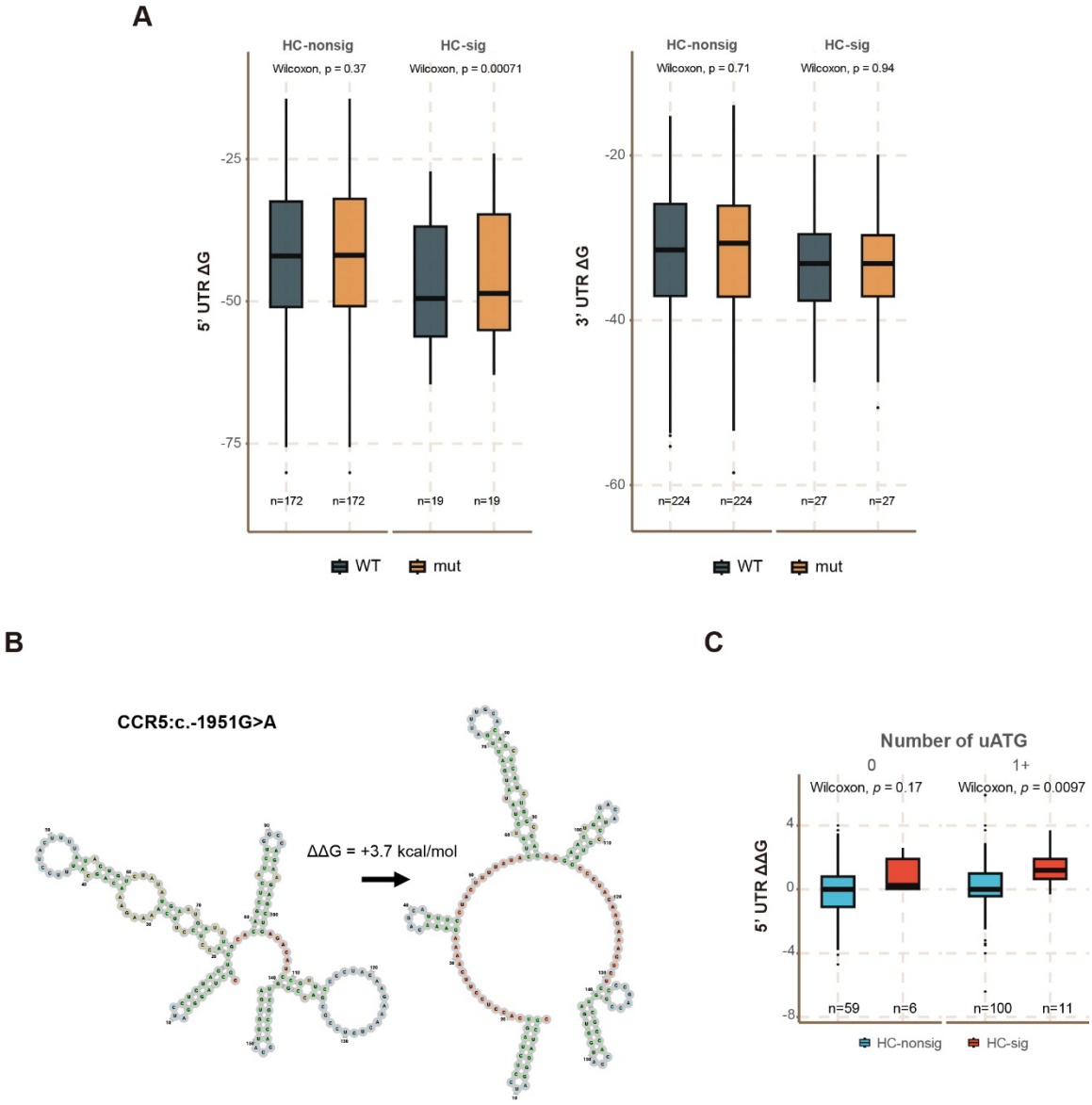

Figure 5. 5' UTR Polysome-shifting mutations elicit structural changes. (A) Significantly weaker folding energy of 5' UTR polysome-shifting variants. The left panel is 5' UTR ΔG and the right panel is 3' UTR ΔG. **(B)** Structural change induced by a CCR5 5' UTR single nucleotide change, as determined by RNAfold. **(C)** Significant differences in ΔΔG values for 5' UTRs that contain upstream ATG (uATG).

Figure 6

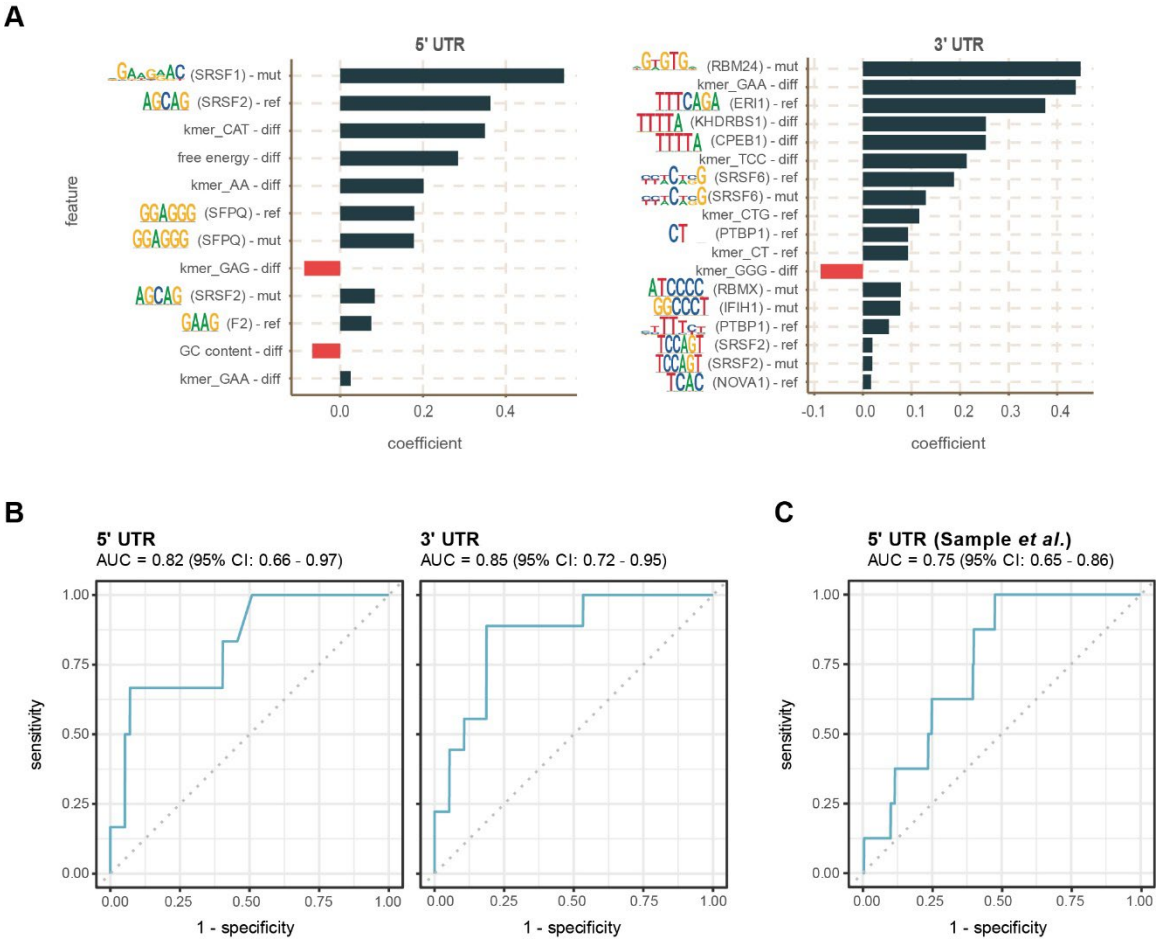

Figure 6. Elastic net model distinguishes polysome-shifting UTR variants. (A) Selected features from elastic net regression explaining the likelihood of a polysome-shifting UTR variant. A positive coefficient indicates a feature that promote polysome shifting, while a negative coefficient suppresses it. "mut" represents a feature of the mutant UTR, "ref" represents a feature of WT UTR, and "diff" indicates the difference (delta) associated with the variant. **(B)** Receiver operating characteristic (ROC) curve for the prediction of polysome-shifting variants on the test set of UTR variants. **(C)** ROC curve for the prediction of polysome-shifting variants on an external dataset of UTR variants (Sample et al., 2019).

Figure 7

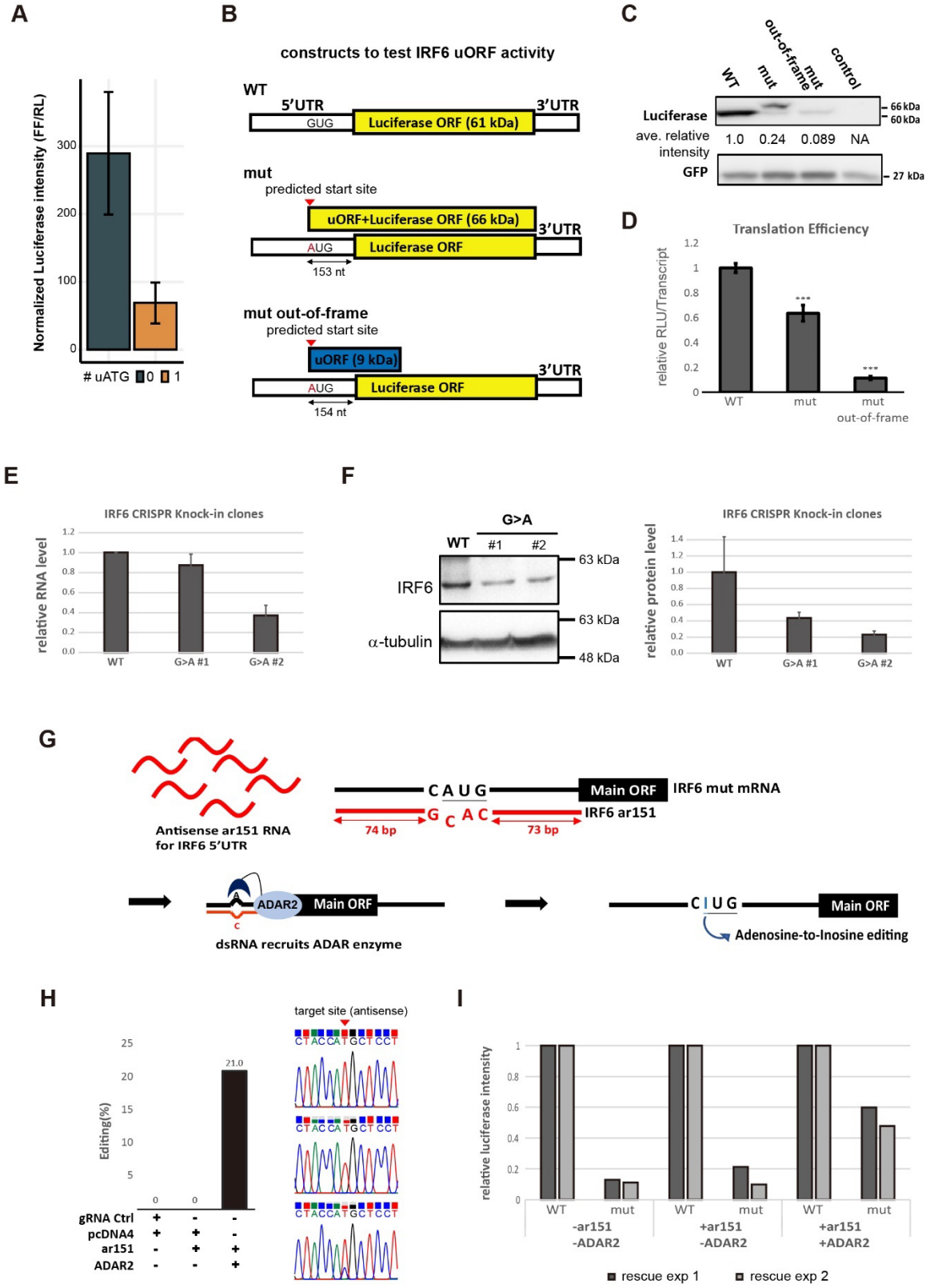
A
Normalized Luciferase intensity (FF/RL)
300
200
100
0
uATG 0 1
B
constructs to test IRF6 uORF activity
WT
5'UTR
GUG
Luciferase ORF (61 kDa)
3'UTR
mut
predicted start site
uORF+Luciferase ORF (66 kDa)
AUG
Luciferase ORF
153 nt
mut out-of-frame
uORF (9 kDa)
154 nt
C
WT
mut
out-of-frame mut
control
Luciferase
66 kDa
60 kDa
ave. relative intensity
1.0 0.24 0.089 NA
GFP
27 kDa
D
Translation Efficiency
relative RLU/Transcript
WT
mut
mut out-of-frame
E
IRF6 CRISPR Knock-in clones
relative RNA level
WT
G>A #1
G>A #2
F
G>A
WT #1 #2
IRF6
63 kDa
α-tubulin
63 kDa
48 kDa
IRF6 CRISPR Knock-in clones
relative protein level
G
Antisense ar151 RNA for IRF6 5'UTR
C A U G
Main ORF
IRF6 mut mRNA
G C A C
IRF6 ar151
74 bp
73 bp
ADAR2
Main ORF
dsRNA recruits ADAR enzyme
C I U G
Main ORF
Adenosine-to-Inosine editing
H
target site (antisense)
Editing(%)
21.0
gRNA Ctrl
pcDNA4
ar151
ADAR2
I
relative luciferase intensity
WT mut
-ar151 -ADAR2
+ar151 -ADAR2
+ar151 +ADAR2
rescue exp 1
rescue exp 2

Figure 7. 5' UTR mutations cause translation inhibition by generating upstream ATG (A) Luciferase activity of eight UTRs with or without a uATG in the 5' UTR. Error bars represent standard errors. **(B)** Constructs of the mutant IRF6 5' UTRs. Mutant (mut) IRF6 generates an in-frame luciferase protein from an upstream ATG, whereas the uORF and luciferase are coded in different frames for the out-of-frame mutant (mut out-of-frame). **(C)** Western blots showing a reduction in luciferase protein levels following 5' UTR mutations. **(D)** Luciferase assays showing a reduction in translation efficiency due to 5' UTR mutations. RLU: relative luminescence units. The individual assays were repeated three times. Statistical significance was determined by a two-tailed Student t-test against WT: ***: $p < 0.001$. **(E)** Relative expression of IRF6 RNA in CRISPR knock-in HEK293T cells. The G>A clones carry the IRF6:c.-4609G>A variant. IRF6 RNA expression was assessed by four independent RT-qPCR experiments and normalized to GAPDH. The error bars represent standard errors. **(F)** IRF6 protein expression in CRISPR knock-in clones. The bar graphs summarize three independent Western blot analyses of IRF6, with normalization to α-tubulin protein levels. The error bars represent standard errors. **(G)** Design of guided ADAR-mediated editing to remove a uORF. **(H)** Editing efficiency achieved by guided ADAR, as determined by Sanger sequencing. **(I)** Restoration of translation efficiency by means of guided ADAR editing, as determined by luciferase assays.